Volume 14, Issue 3, 142433 (1-24)

Iranian Journal of Catalysis (IJC)

https://doi.org/10.57647/j.ijc.2024.1403.33

Preparation, characterization, and antioxidant activity of novel metal (Mn (II), Ni (II), Pd (II), Pt (IV)) complexes: Application of Pd complex in Suzuki-Miyaura cross-coupling reaction

Areeg M. Fadhel[1], Abbas Ali Salih Al-Hamdani[2,*]

[1]*Al-Rusafa, Baghdad Education Directorate, Ministry of Education, Baghdad, Iraq.*
[2]*Department of Chemistry, College of Science for Women, University of Baghdad, Baghdad, Iraq.*

Corresponding author: abbasas_chem@csw.uobaghdad.edu.iq

Original Research

Received:
17 June 2024
Revised:
31 August 2024
Accepted:
10 September 2024
Published online:
17 September 2024

Abstract:

A novel azo dye was synthesized by reacting the N_2^+ (diazonium) salt derived from 2,4,6-trihydroxyacetophenone with 3-aminophenol. The resulting dye was thoroughly characterized using various analytical techniques including micro elemental analysis, Fourier-transform-infrared spectroscopy, electronic spectra, ^{1}H NMR and ^{13}C NMR spectrum, liquid chromatography-mass spectrum, Thermogravimetric analysis (TGA), and Differential Scanning Calorimetry (DSC) for the ligand. Subsequently, the dye was employed to prepare a series of complexes by reacting it with Ni (II), Pt (IV), Pd (II), and Mn (II) ions. These complexes were also subjected to comprehensive characterization, and their geometric shapes were determined using techniques such as micro elemental analysis, Fourier-transform-infrared spectroscopy, electronic spectra, proton NMR spectrum, liquid chromatography-mass spectrum, DSC, magnetic moment, conductivity, and chloride content. The results indicated that the complexes exhibited an octahedral shape, except for the palladium complex which displayed a square planar shape. Notably, the palladium complex was found to be conductive, while the other complexes were non-conductive. The nickel complex exhibited a tetrahedral shape. Furthermore, the synthesized compounds were evaluated for their antioxidant activity, and the IC_{50} value was determined using Ascorbic acid as a standard substance and DPPH as a free radical. The results revealed that the azo dye (H_4L) exhibited higher antioxidant activity compared to ascorbic acid, followed by the Pt-complex, Mn-complex, and Ni-complex. Additionally, the Pd-complex was investigated in a Suzuki-cross coupling reaction. Lastly, all of the metal complexes were optimized using DFT calculation.

Keywords: Metal complex; Catalyst; Suzuki reaction; Antioxidant; Characterization

1. Introduction

Transition-metal-catalyzed cross-coupling reactions have been acknowledged for their significance well before the Nobel Prize in chemistry was awarded in 2010 [1, 2]. These reactions serve as a flexible approach for creating carbon-carbon bonds in contemporary organic synthesis [3–5]. Comprehending the configuration and operation of the genuine active site during catalysis, particularly in the context of organometallic catalysts, is crucial for developing exceptionally efficient catalysts and clarifying the catalytic process and its practical uses. Despite significant endeavors, there persist obstacles in accurately discerning the authentic active sites that undergo formation and transformation in diverse manners during heterogeneous catalysis. The Suzuki-Miyaura reaction is widely utilized and sought-after in the field of synthetic organic chemistry as a cross-coupling

reaction [6–10]. It does not diminish the value or efficacy of other cross-coupling reactions that involve different organometallic or organoelement compounds. Organoboron compounds, including the highly stable and cost-effective arylboronic acids, are widely utilized in organic synthesis for carbon-carbon bond formation and biaryl synthesis due to their compatibility with a wide range of functional groups [11–14]. Additionally, the ability to use various solvents under mild reaction conditions further contributes to the extensive use of these compounds in organic chemistry. The Suzuki-Miyaura reaction stands as the second most commonly employed reaction in the realm of drug discovery and development. Upon receiving the Nobel Prize in Chemistry in 2010, Suzuki had already overcome the primary hurdles associated with challenging substrates in the Suzuki-Miyaura reaction. Subsequently, the focus of the research shifted towards enhancing the effectiveness of catalytic systems. This led to the development of innovative techniques that aimed to operate with extremely low catalyst loading, eliminate the need for toxic phosphine ligands, or even function without ligands. Additionally, new methods were introduced to carry out reactions in aqueous solutions or in pure water, among other advancements. Figure 1, shows some of the important drugs that prepared using Suzuki-cross coupling reaction.

In migratory transformations, nickel and palladium catalysis has been observed to display exceptional performance, as reported recently [15–17]. Over the last ten years, significant attention has been focused on investigating the mechanisms involved in the nickel-catalyzed cross-coupling of alkyl electrophiles. In certain instances, the proposed catalytic cycles involve either Ni (0/II) or Ni (II/IV) [18–20]. However, it is noteworthy that reactions with a nitrogen-based ligand predominantly exhibit a radical chain process and bonding formation originating from a Ni (III) intermediate. On the contrary, there exists a scarcity of comprehensive studies regarding the operational details of migratory cross-coupling reactions catalyzed by nickel. Prior to 1996, the palladium-catalyzed Suzuki-Miyaura reaction involving arene bromides and iodides demonstrated a wide scope of applicability and remarkable efficiency. Nevertheless, the reactivity of arene chlorides, which are more affordable and easily accessible, was hindered by their low reactivity. This can be attributed to their approximate bond dissociation energies, with C–Cl having a value of 96 kcal · mol^{-1}, C–Br having a value of 81 kcal · mol^{-1}, and C–I having a value of 65 kcal · mol^{-1}. Despite this, there have been a few instances where electron-deficient N-heteroaryl chlorides have been proven to be viable through the utilization of palladium catalysts [21–25]. It is important to highlight that while Ni may have a lower price compared to Pd and other precious metals, it does not rank as the top choice among base metals like Fe and Cu. Ni, a member of the group 10 transition metals, is anticipated to demonstrate chemical characteristics that are on par with or superior to those of Pd. In 2023–2024, the most significant palladium catalysts utilized for the Suzuki reaction were Pd nanoparticle [26], Pd-GAP [27], Pd-Schiff base complex [28], Pd- UiO-66-NH_2 [29], zeolite encapsulated Pd [30], Pd-β-cyclodextrine [31], $[Pd(tmeda)(4\text{-}Spy)]_3(X)_3$ [32], Pd-Isatin-Schiff base@rGO [33], Pd Schiff-base [34], and Pd thiourea organic framework [35].

Free radicals, characterized by the presence of an unpaired electron, are a specific type of reactive species (RS) that play a crucial role in various biological processes such as respiration, metabolism, cell signaling, and numerous other physiological functions. Transition metal complexes with nitrogen-containing ligands hold significant importance in both organic and inorganic chemistry due to their unique magnetic and electrical characteristics. Azo compounds, characterized by their high stability, consist of an azo bridge group (–N=N–) that connects both ends of two

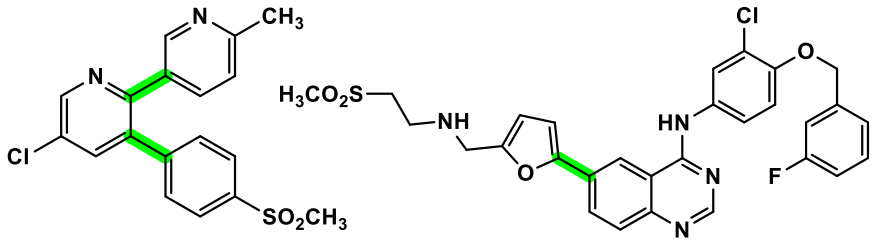

Etoricoxib (Antiinflammatory) *Lapatinib (Anticancer)*

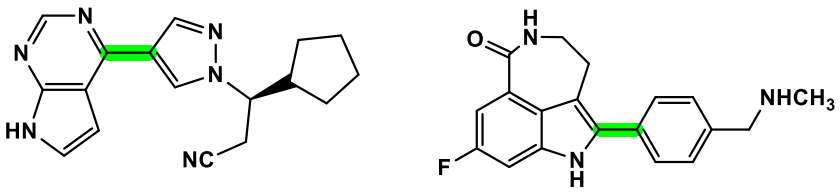

Ruxolitinib (Myelofibrosis) *Rucaparib (Anticancer for phase III)*

Figure 1. Some of the important drugs prepared using Suzuki-cross coupling reaction.

nitrogen atoms to aliphatic or aromatic derivatives. These compounds are widely recognized for their significant role in antioxidant activity and are extensively utilized in various applications. Recently, there has been a growing focus among researchers on the utilization of azo ligands and their connections in medical therapy. These ligands have been incorporated into the production of pharmaceuticals for treating diabetes, infections, and even anti-cancer medications, such as triple gold complexes, due to their significant inhibitory properties. Furthermore, they are valued for their role as antioxidants [36–38].

The study involved the synthesis of a new azo dye which was utilized as a ligand in the formation of complexes with various metal ions such as Ni (II), Pt (IV), Pd (II), and Mn (II). These complexes were further characterized through thermal stability, spectroscopic analysis, and thermal decomposition using TGA and DSC curves. Moreover, the antioxidant properties of the compounds were evaluated by testing their activity against the DPPH radical and comparing it to that of the natural antioxidant Ascorbic acid. Subsequently, the Ni and Pd complexes were employed in the Suzuki-Miyaura cross-coupling reaction.

2. Experimental

2.1 Materials and instruments

The following substances, including absolute ethanol, methanol, dimethyl sulfoxide, and various high purity solvents, were acquired from F-897ewluka and Sigma-Aldrich. Metal salts such as $NiCl_2 \cdot 6H_2O$, $PdCl_2$, $H_2PtCl_6 \cdot 6H_2O$, and $MnCl_2 \cdot 4H_2O$ were supplied by BDH Co. and Sigma-Aldrich Co. DSC and TGA were conducted on the Schiff-base ligand (HL) using the Perkin-Elmer Pyris Diamond instrument. The ^{1}H-NMR study was carried out with the Bruker 400-MHz spectrometer, while elemental microanalysis was performed using the Perkin-Elmer automatic equipment specimen 240-B. Mineral estimation was done using the Shimadzu AA-680G AA spectrometer. Accessibility measures were determined with the Jenway 4071 instrument. Chloride content was estimated gravimetrically. Magnetic properties were measured using the balance magnetic susceptibility model MSR-Mki. Fourier-transform infrared analysis was conducted on the Shimadzu 3800 spectrometer (4000–400 cm^{-1}). Electronic spectral data were obtained using the Shimadzu 160 spectrophotometer. Liquid Chromatography-Mass analysis of compounds was carried out with the LC Mass100P Shimadzu instrument. The ^{1}H and ^{13}C-NMR spectra were acquired using the Bruker 400-MHz spectrometer.

2.2 Typical procedure for the preparation of the azo-dye ligand

The synthesis of the ligand involves a two-step process. Initially, (0.01 mol, 1 g) of 2,4,6-trihydroxyactophenone is dissolved in a 250 mL flask containing a combination of 3 mL of 37 % Hydrochloric acid (HCl) and 35 mL of distilled water (DW) to prepare a diazonium salt. Subsequently, the resulting mixture is cooled to a temperature ranging from 0–5 °C. Afterwards, a cooled mixture is continuously stirred while a solution containing (0.01 mol, 1 g) of sodium nitrite ($NaNO_2$) dissolved in 30 mL of DW is slowly added drop by drop. It is crucial to monitor the temperature during this process to ensure that it does not exceed a 5 °C increase. Following a duration of 30 minutes, the solution is allowed to sit undisturbed for an additional 15 minutes, leading to the production of the (N_2^+) diazonium salt as the end product of the initial phase. In the subsequent stage, a diazotization coupling reaction is carried out by combining the (N_2^+) diazonium salt of 3-aminophenol with a solution involving 2,4,6-trihydroxyactophenone (1.5 g, 0.004 mol) dissolved in 50 mL of absolute EtOH and 15 mL of sodium hydroxide (NaOH, 10 %). This reaction is carried out under continuous stirring while maintaining a cooling environment. Throughout this process, precipitates of different colors are observed and obtained. The proton NMR spectrum reveals specific chemical shifts (ppm) for different protons. The methyl group of the ketone shows a chemical shift of 2.6 δ ppm (3H, Singlet), while the Ar – H protons exhibit a range of 7.5–8.0 δ ppm (5H, multiplet). The protons of the phenolic groups display a chemical shift range of 9.75–9.98 δ ppm (4H, doublet). However, the carbon NMR spectrum acquired with chloroform as the solvent displays discernible peaks at different chemical shifts. These include 178.8 (C1), 137.4 (C2), 165 (C3), 156.2 (C4), 174.0 (C5), 155 (C6), 127.0 (C7), 182.0 (C8), 106.5 (C9), 190.0 (C10), 119.0 (C11), 170.0 (C12), 195.0 (C13), 49.9 (C14).

2.3 Typical procedure for the synthesis of metal complexes

In order to synthesize the targeted complex, Azo ligand (H_4L) (0.005 mol, 5 mmol, 1.44 g) was slowly added and dissolved in 15 mL of absolute EtOH while continuously stirring. This solution was then combined with the precise amount of metal salt ($NiCl_2 \cdot 6H_2O$) (5 mmol) that had been dissolved in 10 mL of water. The resulting mixture was heated and refluxed for a duration of two hours at 60 °C. Subsequently, the mixture was allowed to cool to room temperature and left in a cabinet for 24 hours to ensure complete formation and precipitation. The solution was then filtered, and the residue was washed multiple times with distilled water and a small amount of cold EtOH. Finally, the prepared complex underwent recrystallization using absolute ethanol. Following the same procedure for the synthesis of Nickel complex, complexes of other metal salts, namely [$PdCl_2$, $H_2PtCl_6 \cdot 6H_2O$, and $MnCl_2 \cdot 4H_2O$], were prepared. These salts were dissolved in 10 mL of water, and Azo ligand (H_4L, 0.1 g, 0.4 mmol) in 15 mL of EtOH was added gradually. The mixtures were then heated and refluxed for approximately two hours at 40 °C. The resulting complex precipitates were isolated, and impurities were removed by partially dissolving in hot ethanol. The complexes were then dried and weighed accordingly. Based on the atomic absorption spectroscopy calculation, the total amount of Pd on complex was estimated approximately 32 wt% or 3.0 mmol/g of Pd-complex.

2.3.1 General procedure for the synthesis of target molecules from Suzuki-Miyaura cross-coupling reaction

In a 25 mL round bottom flask equipped with a condenser and magnetic stirring bar, aryl halide (5.0 mmol), phenyl boronic acid (6.0 mmol), Pd (II)-complex (50 mg), K_2CO_3 (10.0 mmol), and H_2O (6.0 mL) were combined. The mixture was then heated at reflux while the progress of the reaction was monitored using TLC until complete conversion of the aryl halide was confirmed. Once the reaction was complete, a mixture of 5.0 mL of hot water, 5.0 mL of ethyl acetate, or 5.0 mL of dichloromethane (for compounds 7–9) was added to the reaction mixture. The catalysts were separated using a filter sintered-glass with mesh grade-4. The resulting organic solution was then evaporated on a rotary evaporator, yielding the crude product. The crude product underwent purification through column chromatography, utilizing a hexane/ethyl acetate elution, resulting in a pure product.

2.4 Reusability of the catalyst

The investigation focused on the recyclability of the current catalysts in the Suzuki-Miyaura coupling reaction involving 4-iodoanisole and phenylboronic acid. Once the reactions were finished, the catalysts were retrieved through a straightforward filtration process, then rinsed with DMF, H_2O, diethyl ether, acetone, and finally dried under reduced pressure at 60 °C. These regenerated catalysts were utilized in subsequent runs with new batches of 4-iodoanisole and phenylboronic acid.

2.5 Physical and spectroscopic data for target product

1,1′-Biphenyl (Compound 1): M.p.: 69–71 °C, IR (KBr), ν (cm^{-1}): 3032, 1566, 1476. ^{1}H NMR (400 MHz, $CDCl_3$): δ (ppm) 7.32–7.37 (2H, m), 7.44 (4H, triplet, $J = 7.1$ Hz), 7.60 (4H, doublet, $J = 8.1$ Hz). Note: The identification of compounds in entries 2 and 3 were provided using melting point and FT-IR spectrum.

4-Methoxy-1,1′-biphenyl (Compound 2): M.p.: 88–90 °C, IR (KBr), ν (cm^{-1}): 3059, 3054, 2958, 1604, 1484, 1248, 1035. ^{1}H NMR (400 MHz, $CDCl_3$): δ (ppm) 3.84 (3H, singlet), 6.97 (2H, doublet, $J = 8.3$ Hz), 7.29 (1H, triplet, $J = 7.5$ Hz), 7.41 (2H, triplet, $J = 7.4$ Hz), 7.54 (4H, triplet, $J = 7.5$ Hz). Note: The identification of compounds in entries 5 and 6 were provided using melting point and FT-IR spectrum.

2-Methoxy-1,1′-biphenyl (Compound 3): M.p.: oil like, IR (KBr), ν (cm^{-1}): 3058, 2931, 1596, 1480, 1258, 1027. ^{1}H NMR (400 MHz, $CDCl_3$): δ (ppm) 3.77 (3H, singlet), 6.97 (1H, doublet, $J = 8.6$ Hz), 7.01 (1H, triplet, $J = 8.7$ Hz), 7.27–7.33 (3H, multiplet), 7.39 (2H, triplet, $J = 7.1$ Hz), 7.52 (2H, doublet, $J = 5.1$ Hz). Note: The identification of compounds in entries 8 and 9 were provided using melting point and FT-IR spectrum.

4-Phenylphenol (Compound 4): M.p.: 157–160 °C, IR (KBr), ν (cm^{-1}): 3405, 3035, 1602, 1485. ^{1}H NMR (400 MHz, $CDCl_3$): δ (ppm) 6.92 (2H, doublet, $J = 8.3$ Hz), 7.32 (1H, triplet, $J = 7.3$ Hz), 7.43 (2H, triplet, $J = 7.5$ Hz), 7.50 (2H, doublet, $J = 8.3$ Hz), 7.55 (2H, triplet, $J = 7.1$ Hz), 8.27 (1H, doublet, $J = 6.7$ Hz). Note: The identification of compounds in entries 11 and 12 were provided using melting point and FT-IR spectrum.

4-Phenylbenzaldehyde (Compound 5): M.p.: 57–58 °C, IR (KBr), ν (cm^{-1}): 3065, 1709, 1587, 1475, 764, 690. ^{1}H NMR (400 MHz, $CDCl_3$) δ (ppm): 7.44 (1H, triplet, $J = 6.9$ Hz), 7.52 (2H, triplet, $J = 7.0$ Hz), 7.76 (2H, doublet, $J = 7.7$ Hz), 7.90 (2H, doublet, $J = 7.7$ Hz), 7.98 (2H, doublet, $J = 8.1$ Hz), 10.06 (1H, singlet, CHO). Note: The identification of compounds in entries 14 and 15 were provided using melting point and FT-IR spectrum.

3. Results and discussion

3.1 Preparation and characterizations of the metal complexes

The novel ligand, (E)-1-(2,4,6-trihydroxy-3-((3-hydroxyphenyl)diazenyl)phenyl)ethan-1-one, was synthesized via a two-step synthetic route outlined in Scheme 1. Initially, the preliminary ligand was synthesized by reacting 3-aminophenol with $NaNO_2$ and HCl in an aqueous medium, resulting in the formation of diazonium chloride salt. During the second stage of synthesizing the H_4-ligand, the outcome of the initial step underwent a reaction with 1-(2,4,6-trihydroxyphenyl)ethan-1-one in the existence of sodium hydroxide, resulting in the desired ligand.

After preparation of target ligand, the metal complexes were synthesized according to the Scheme 2. In order to synthesize the desired complex, the Azo ligand was introduced and dissolved in absolute ethanol. Subsequently, this solution was combined with a specific amount of metal salts [$NiCl_2 \cdot 6H_2O$, $PdCl_2$, $H_2PtCl_6 \cdot 6H_2O$, and $MnCl_2 \cdot 4H_2O$] that had been dissolved in 10 mL of water. The resulting mixture was then subjected to heating and refluxing for a duration of two hours at a temperature range of 40–60 °C. Following this step, the mixture was allowed to cool down to room temperature and stored in a cabinet for a period of 24 h to facilitate complete formation and precipitation. The solution was then filtered, and the solid residue was washed multiple times with distilled water and a small amount of cold ethanol. Finally, the synthesized complex was purified through recrystallization using absolute ethanol.

The characterization of the ligand's preparation was confirmed through the utilization of the ^{1}H NMR and ^{13}C NMR techniques. The synthesized ligand's ^{1}H NMR and ^{13}C NMR are illustrated in Figure 2 and Figure 3, respectively.

The current investigation effectively determined the existence of carbon (C), hydrogen (H), nitrogen (N), and oxygen (O) in both the ligand (H_4L) and its corresponding complexes. This verification was supported by the data presented in Table 1, indicating that the identification through this method aligned well with the expected values. Additionally, the metal ratios were determined utilizing the AAS technique. The results obtained from both methodologies exhibited a high level of consistency with the theoretical predictions, as illustrated in Table 1.

The mass spectrum of the ligand (H_4L) depicted in Figure 4

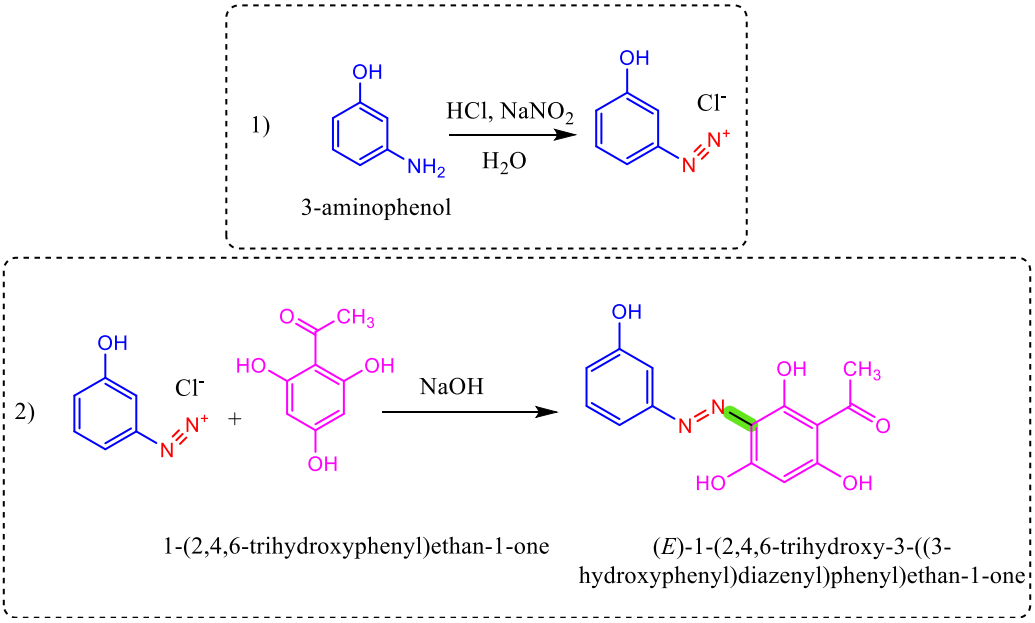

Scheme 1. Typical route for the synthesis of azo dye ligand.

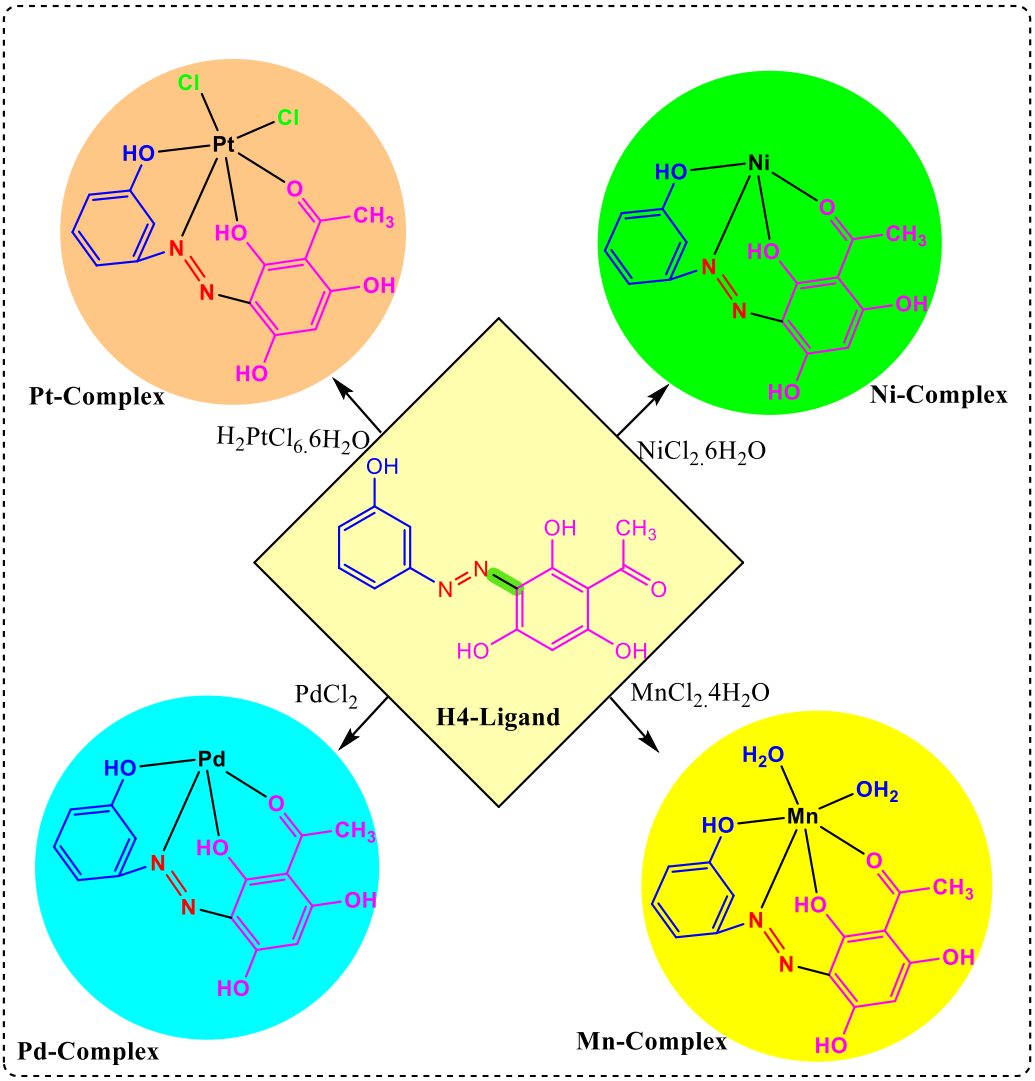

Scheme 2. An artificial route for the production of metal complexes.

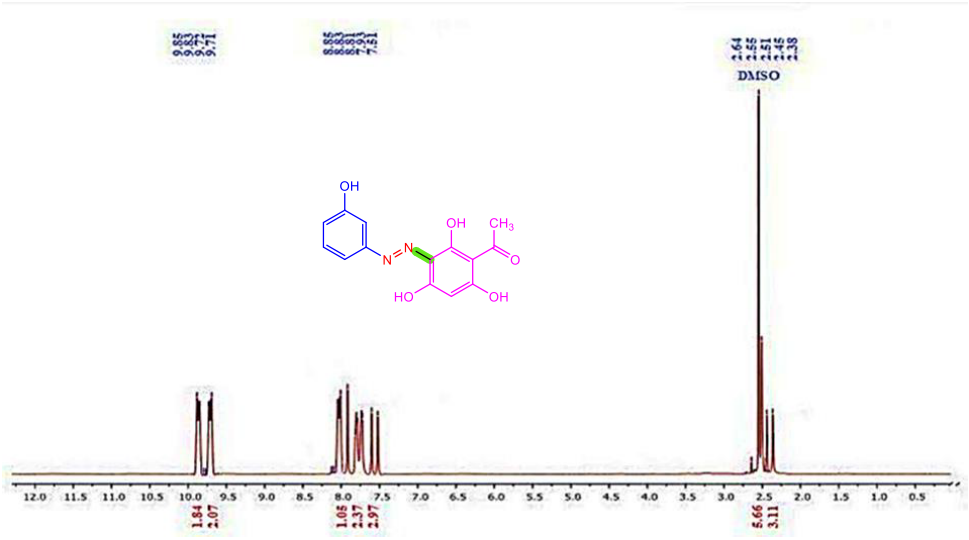

Figure 2. ^{1}H NMR spectrum of H_4-ligand.

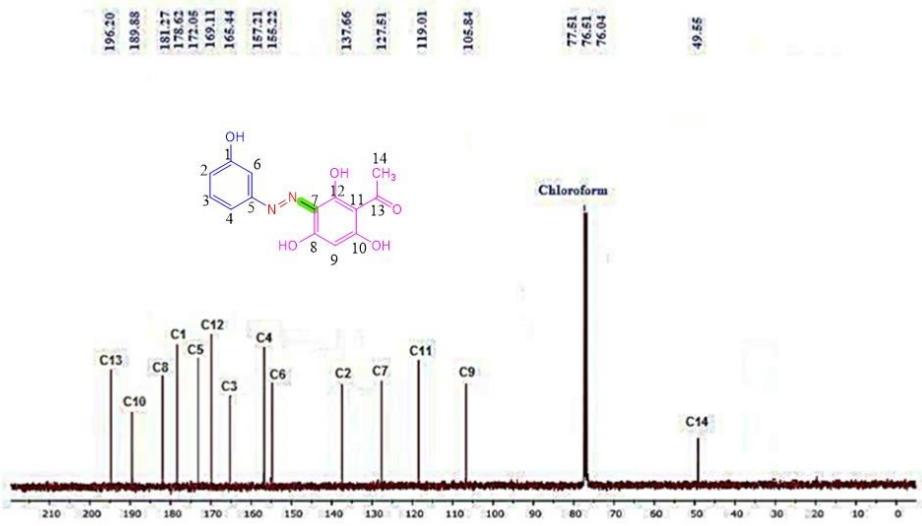

Figure 3. ^{13}C NMR spectrum of H_4-ligand.

Table 1. The necessary data for micro-elemental analysis, physical characteristics, metal ratio, and chloride content.

Entry	Compound (M. wt)	Percentages of elements found through microanalysis (calculated)					Yield (%)	m.p °C	Colour
		Carbon	Hydrogen	Nitrogen	Metal	Cl			
1	$C_{14}H_{12}N_2O_5$ 288.26	57.89 (58.33)	4.67 (4.20)	10.11 (9.72)	–	–	80	146–148	Brown
2	$C_{14}H_{14}N_2O_7Mn$ 377.21	45.21 (44.58)	3.01 (3.74)	8.41 (7.43)	14.97 (14.56)	–	73	172–174	Light brown
3	$C_{14}H_{10}N_2O_5Ni$ 344.93	48.84 (48.75)	3.83 (2.92)	9.11 (8.12)	16.69 (17.02)	Nil* –	76	194–196 dec.	Dark green
4	$C_{14}H_{10}N_2O_5Pd$ 392.66	41.97 (42.82)	3.22 (2.57)	8.01 (7.13)	26.83 (27.10)	–	72	212–214 dec.	Dark brown
5	$C_{14}H_{10}N_2O_5Cl_2Pt$ 552.22	31.13 (30.45)	2.54 (1.83)	6.01 (5.07)	34.82 (35.33)	11.94 (12.84)	81	204–206 dec.	Reddish brown

* Nil: negative or very trace near zero.

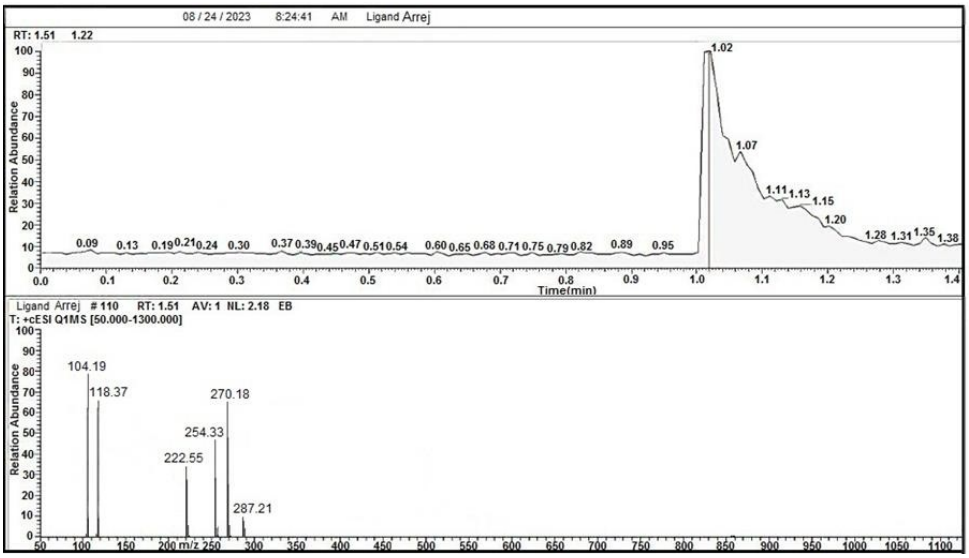

Figure 4. Liquid chromatography-Mass (LC-Mass) spectra of H_4-ligand.

and Scheme 3 reveals the molecular ion pattern (M^+) for $C_{14}H_{11}N_2O_5$ at 287 m/z. This value corresponds to the calculated molar mass of the prepared azo-moiety, and the fragmentation patterns observed in the spectrum further support this finding. Specifically, the spectrum displays the presence of fragment ions such as $C_{14}H_{10}N_2O_4^+$ at 270.24 m/z, $C_{14}H_{10}N_2O_3^+$ at 254.24 m/z, $C_{14}H_{10}N_2O^+$ at 222.24 m/z, $C_8H_6O^+$ at 118.13 m/z, and $C_6H_4N_2^+$ at 104.11 m/z [39].

Moving on to Figure 5 and Scheme 4, the platinum complex exhibits a prominent peak at 552 m/z, corresponding to the molecular ion (M^+). Additionally, several other peaks are observed, including $C_{14}H_{10}PtN_2O_4$ at 465.00 m/z, $C_{12}H_8PtN_2O_3$ at 423.28 m/z, $C_{12}H_8PtN_2O_2$ at 407.28 m/z, PtN_2 at 223.09 m/z, $C_6H_4O_2$ at 108.09 m/z, and C_6H_4 at 76.10 m/z. It is worth noting that all the experimental results obtained are in excellent agreement with the theoretical predictions, providing strong evidence for the formation of the ligand and its complexes [39].

The UV-Vis curve of the H_4L ligand and its complexes, as illustrated in Figure 6, reveals a moderately wide absorption peak at 300 nm, corresponding to 33333 cm^{-1}, which is attributed to the ($\pi \rightarrow \pi^*$) electronic transition. Additionally, there are other broad peaks at 391 nm, equivalent to 25575 cm^{-1}, associated with the $n \rightarrow \pi^*$ electronic transition [40]. The nickel complex exhibits a spectrum with transitions at specific wavelengths and corresponding energy levels. These transitions include two $\pi \rightarrow \pi^*$ transitions, $n \rightarrow \pi^*$ transition, and a charge transfer transition from metal to ligand (C. T M $\longrightarrow$ L). The wavelengths and energy levels associated with these transitions are as follows: (40000 cm^{-1}, 250 nm, and 34482 cm^{-1}, 290 nm), (32257 cm^{-1}, 310 nm), and (29411 cm^{-1}, 340 nm). The ligand undergoes transitions resulting in shifts in their wavelengths due to coordination with the metal. Notably, the d-d transitions occurring in the visible region at 507 nm (20000 cm^{-1}) and 572 nm (18181 cm^{-1}) correspond to $^3T_{1(F)} \longrightarrow {}^3T_{2(F)}$ and $^3T_{1(F)} \longrightarrow {}^3A_2$, respectively [41]. The platinum complex exhibits two transitions in the UV region, as indicated by its UV-Vis spectrum. These transitions occur at wavelengths of 230 nm and 290 nm, corresponding to energy values of 34478 cm^{-1} and 34482 cm^{-1}, respectively. The first transition is attributed to a $\pi \rightarrow \pi^*$ transition, while the second transition is associated with an $n \rightarrow \pi^*$ transition. Furthermore, there are d-d transitions occurring in the visible spectrum at specific wavelengths and corresponding energy levels. These transitions are observed at (24096 cm^{-1}, 415 nm), (16949 cm^{-1}, 590 nm), (600 nm, 16666 cm^{-1}), and (630 nm, 15873 cm^{-1}). These transitions can be attributed to $n \rightarrow \pi^* + C.T$ (M $\longrightarrow$ L), $^1A_{1g} \longrightarrow {}^1T_{2g}$, $^1A_{1g} \longrightarrow {}^1T_{1g}$, and $^6A_{1g} \longrightarrow {}^1T_{3g}$, respectively. The UV-Vis spectrum of the palladium complex exhibits two distinct peaks in the UV region: (290 nm, 34484 cm^{-1}) and (350 nm, 28571 cm^{-1}). These peaks correspond to the $\pi \rightarrow \pi^*$ and $n \rightarrow \pi^*$ transitions, respectively. The subsequent maxima in the observable spectrum at wavelengths of 410 nm (24390 cm^{-1}) and 570 nm (17543 cm^{-1}) are attributed to transitions from $^1A_{1g}$ to $^1B_{1g}$ and $^1A_{1g}$ to $^1A_{2g}$, respectively [42]. The manganese complex exhibits two transitions in the UV-visible spectrum, specifically at wavelengths of 245 nm and 300 nm, corresponding to energy values of 40816 cm^{-1} and 33333 cm^{-1}, respectively. These transitions can be attributed to the $\pi \rightarrow \pi^*$ and $n \rightarrow \pi^*$ transitions, respectively. Furthermore, there are d-d transitions occurring in the visible spectrum at the following wavelengths and wavenumbers: (430 nm, 23255 cm^{-1}), (500 nm, 20000 cm^{-1}), (580 nm, 17241 cm^{-1}), and (590 nm, 16949 cm^{-1}). These transitions correspond to specific electronic configurations, namely C. T (M $\longrightarrow$ L), $^6A_{1g} \longrightarrow {}^4E_{g(G)}$, $^6A_{1g} \longrightarrow {}^4T_{2g(G)}$, and $^6A_{1g} \longrightarrow {}^4T_{1g(G)}$, respectively. All complexes demonstrate identical absorption bands observed in the ligand at the UV region, albeit with certain alterations resulting from the coordinative binding with metal ions [43, 44].

Furthermore, the spectra also showcase novel absorption peaks within the visible spectrum, specifically attributed

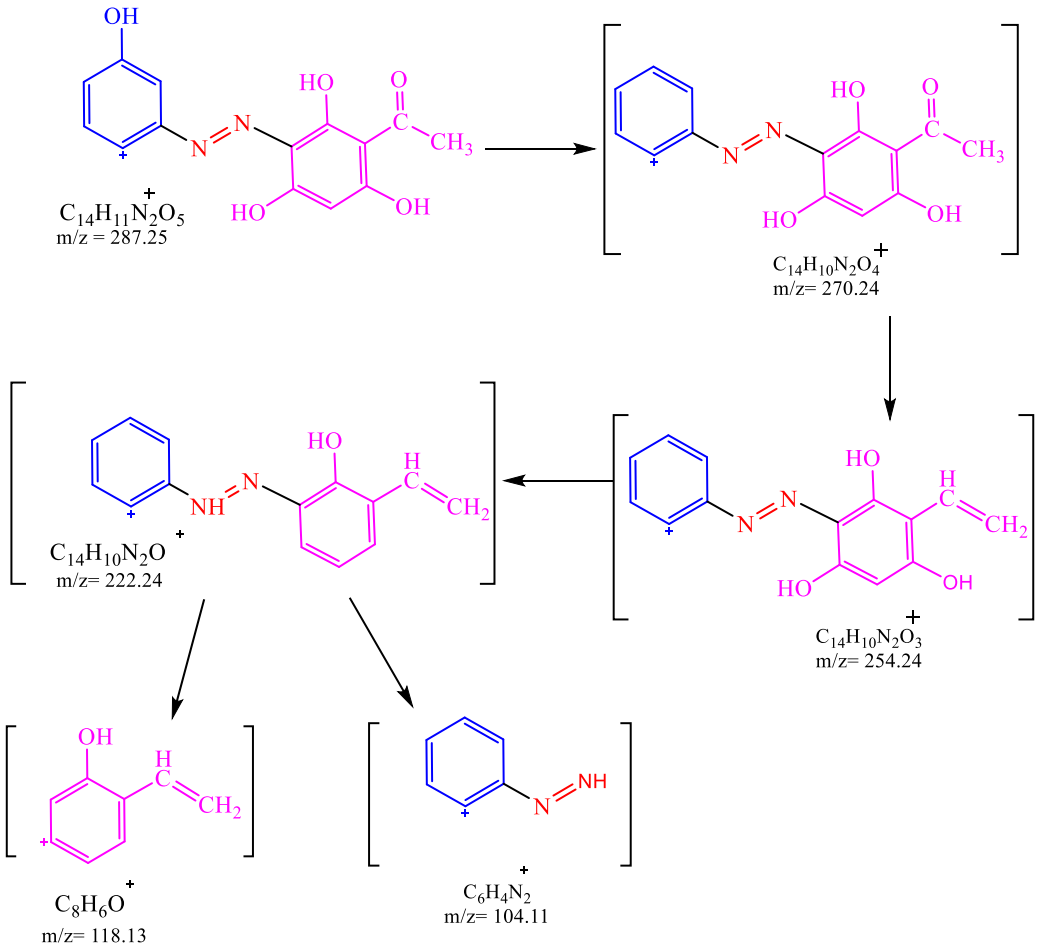

Scheme 3. The fragmentation of H_4-ligand for mass spectroscopy.

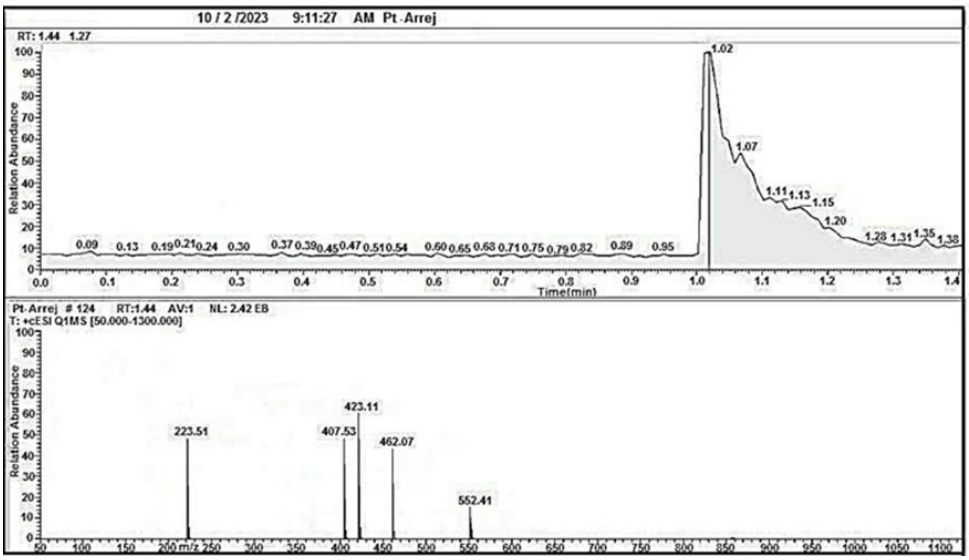

Figure 5. Liquid chromatography-Mass (LC-Mass) spectra of Pt-complex.

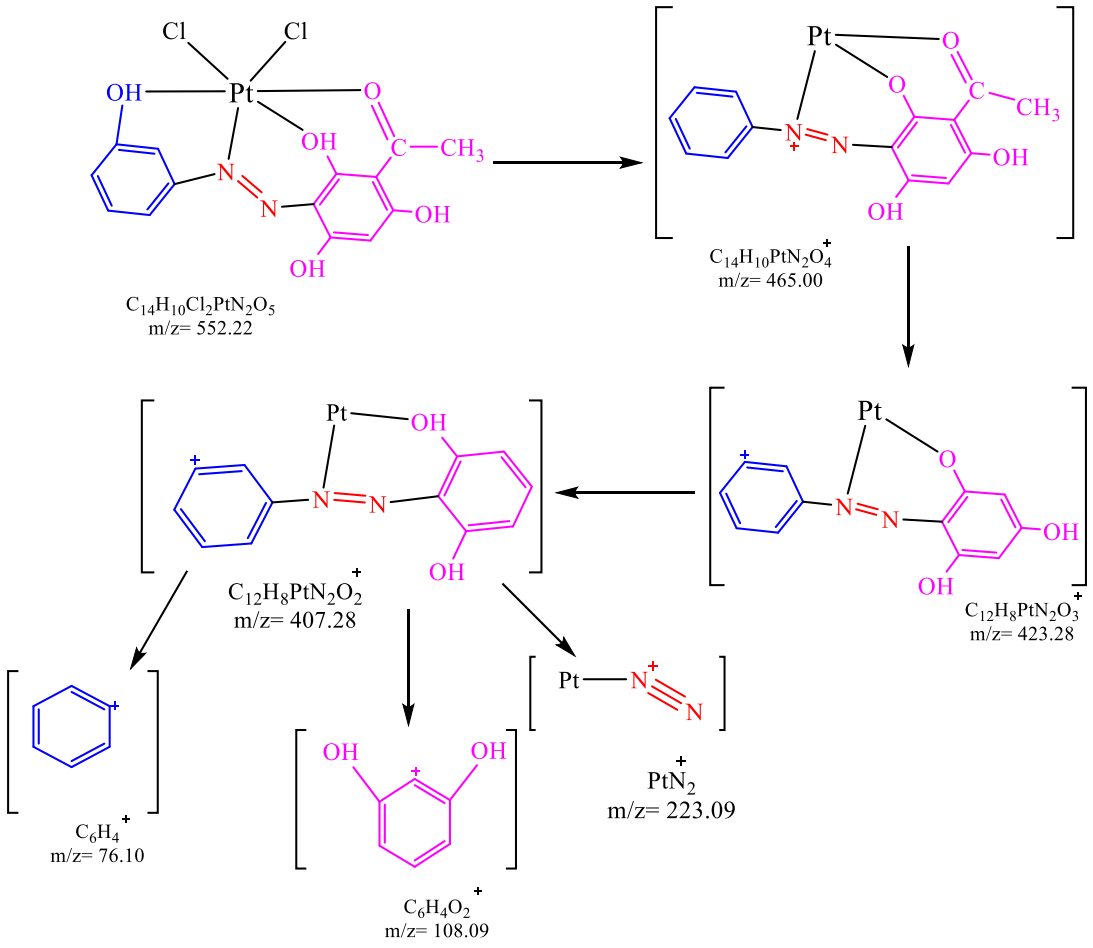

Scheme 4. The fragmentation of Pt-complex for mass spectroscopy.

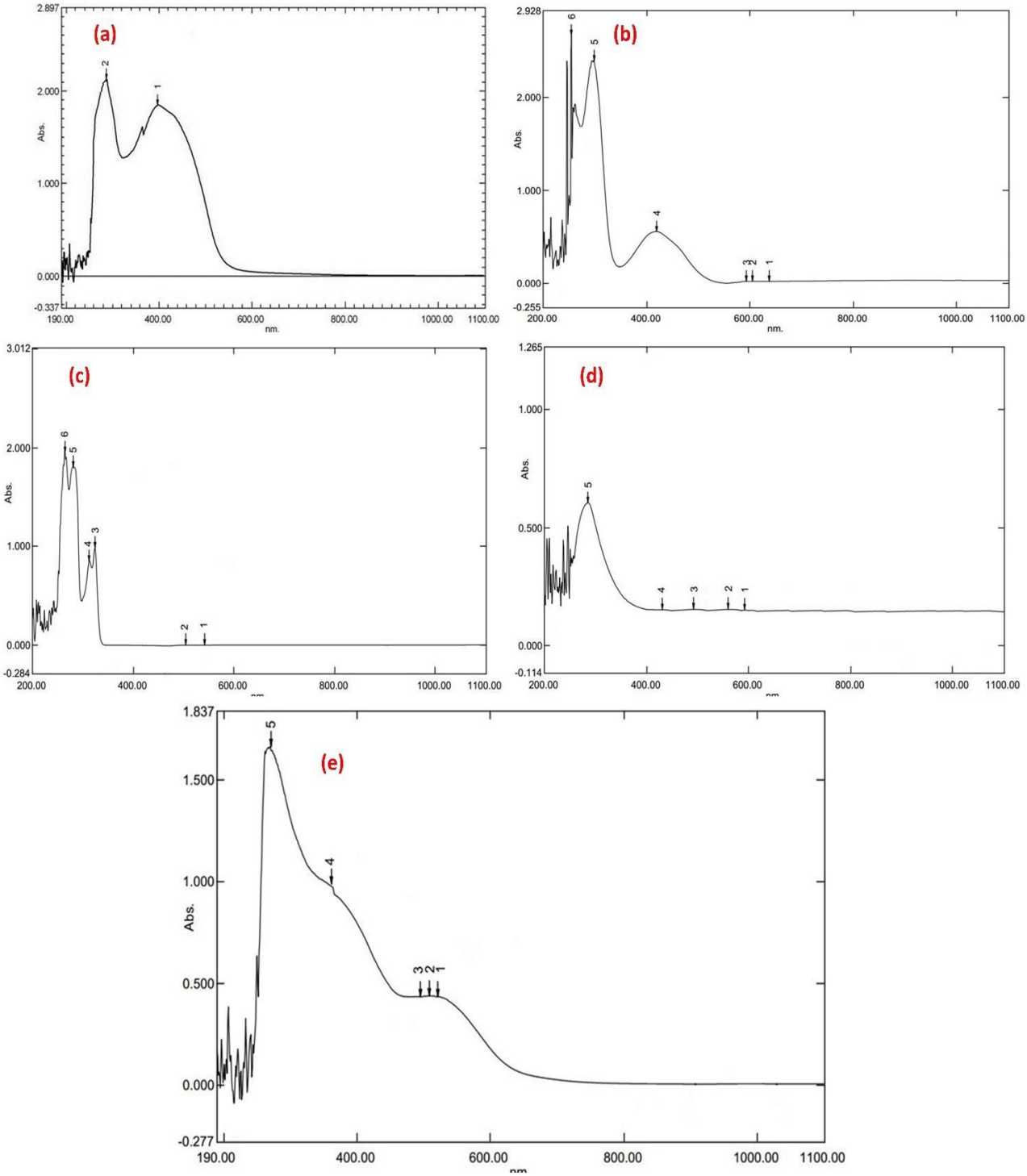

Figure 6. UV-Vis spectra of a) H_4-ligand, b) Pt-complex, c) Ni-complex, d) Mn-complex, and e) Pd-complex.

to d-d transitions, as outlined in Table 2. The molar conductance of the complex solutions that were prepared was calculated by diluting the complexes to a concentration of 10^{-3} M in DMSO solvent at room temperature. The measurements provided in Table 2 correspond to the suggested structural formula of the complexes, affirming their non-electrolyte characteristics and verifying the geometries of the acquired complexes. Magnetic susceptibility measurements are widely used in diagnosing and studying complex transition metals. The main emphasis in this field revolves around the implications of having incompletely filled outer shells with electrons; magnetic evaluations offer understanding into the electronic structure of the compound and the oxidation state of transition metal atoms, whereas the existence of unpaired electrons in a transition metal ion indicates the spin state of the complex being studied, whether it is in a low or high spin state.

The DSC technique, also known as DSC, is a pyrolysis method utilized to analyze the thermal changes and determine the absorbed and released temperatures in a tested substance [45]. This method is utilized in a wide range of industries including minerals, organic compounds, pharmaceuticals, polymers, inorganic substances, and food, allowing for the evaluation of their purity and stability [46]. In a recent study, a thermal analysis was conducted on a ligand and several complexes using TGA and DSC curves. The obtained results, presented in Table 3 and Figure 7, include the Ti/°C (initial temperature), Tf/°C (final temperature), and heat amount (ΔH) measured in J/g units, indicating whether the process was exothermic or endothermic [47].

Additionally, the thermal behavior of the ligand (H_4-L) and its complexes was characterized using a TGA curve, as shown in Figure 8. This method entails observing the alteration in mass of a substance in relation to temperature, while implementing a regulated thermal schedule within a

Table 2. The ligand (H_4L) and its complexes are studied by UV-Vis.

Entry	**Compounds Geometries**	**Abs.**	λ_{max}	ν **cm**$^{-1}$	μ_{eff} **B.M**	**Molar cond. S.** **cm**$^2 \cdot$**mol**$^{-1}$	**Transition**
1	$C_{14}H_{12}N_2O_5$ (H_4L)	2.090	300	33333	–	–	$\pi \rightarrow \pi^*$
		1.850	391	25575			$n \rightarrow \pi^*$
2	$C_{14}H_{10}N_2O_5Ni$ Tetrahedral	1.980	250	40000	3.37	8	$\pi \rightarrow \pi^*$
		1.950	290	34482			$\pi \rightarrow \pi^*$
		0.750	310	32257			$n \rightarrow \pi^*$
		0.800	340	29411			CT (M $\longrightarrow$ L)
		0.100	507	20000			$^3T_{1(F)} \longrightarrow {}^3T_{2(F)}$
		0.100	572	18181			$^3T_{1(F)} \longrightarrow {}^3A_2$
3	$C_{14}H_{10}N_2O_5Cl_2Pt$ Octahedral	2.890	230	43478	diamagnetic	12	$\pi \rightarrow \pi^*$
		2.555	290	34482			$n \rightarrow \pi^*$
		0.500	415	24096			$n \rightarrow \pi^* + C.T \longrightarrow L$
		0.200	590	16949			$^1A_{1g} \longrightarrow {}^1T_{2g}$
		0.200	600	16666			$^1A_{1g} \longrightarrow {}^1T_{1g}$
		0.200	630	15873			$^1A_{1g} \longrightarrow {}^1T_{3g}$
4	$C_{14}H_{10}N_2O_5Pd$ Square planer	1.600	290	34484	diamagnetic	9	$\pi \rightarrow \pi^*$
		0.999	350	28571			$n \rightarrow \pi^*$
		0.400	460	21739			$^1A_{1g} \longrightarrow {}^1B_{1g}$
		0.400	570	17543			$^1A_{1g} \longrightarrow {}^1A_{2g}$
5	$C_{14}H_{10}N_2O_5Cl_2Mn$ Octahedral	0.623	245	40816	5.21	12	$\pi \rightarrow \pi^*$
		0.510	300	33333			$n \rightarrow \pi^*$
		0.127	430	23255			C.T M $\longrightarrow$ L
		0.126	500	20000			$^6A_{1g} \longrightarrow {}^4E_{g(G)}$
		0.126	580	17241			$^6A_{1g} \longrightarrow {}^4T_{2g(G)}$
		0.125	590	16949			$^6A_{1g} \longrightarrow {}^4T_{1g(G)}$

Table 3. Differential scanning calorimetry data for ligand and some complexes.

Entry	Compound	Ti/°C	Tf/°C	Max. T. point °C	ΔH J/g	ΔS J	ΔG J	Type
1	$C_{14}H_{12}N_2O_5$ (H_4L) 288.26	387.65	395.13	392.40	−3.43	−0.0087	176.603	Exothermic
2	$C_{14}H_{10}N_2O_5Cl_2Pt$ 391.70	43.76	108.80	74.42	184.62	2.48	0.0584	Exothermic
		218.42	357.93	288.99	249.39	0.86	0.8586	Exothermic
3	$C_{14}H_{10}N_2O_5Pd$ 392.66	68.27	127.77	98.27	−91.07	−0.926	−0.0719	Endothermic

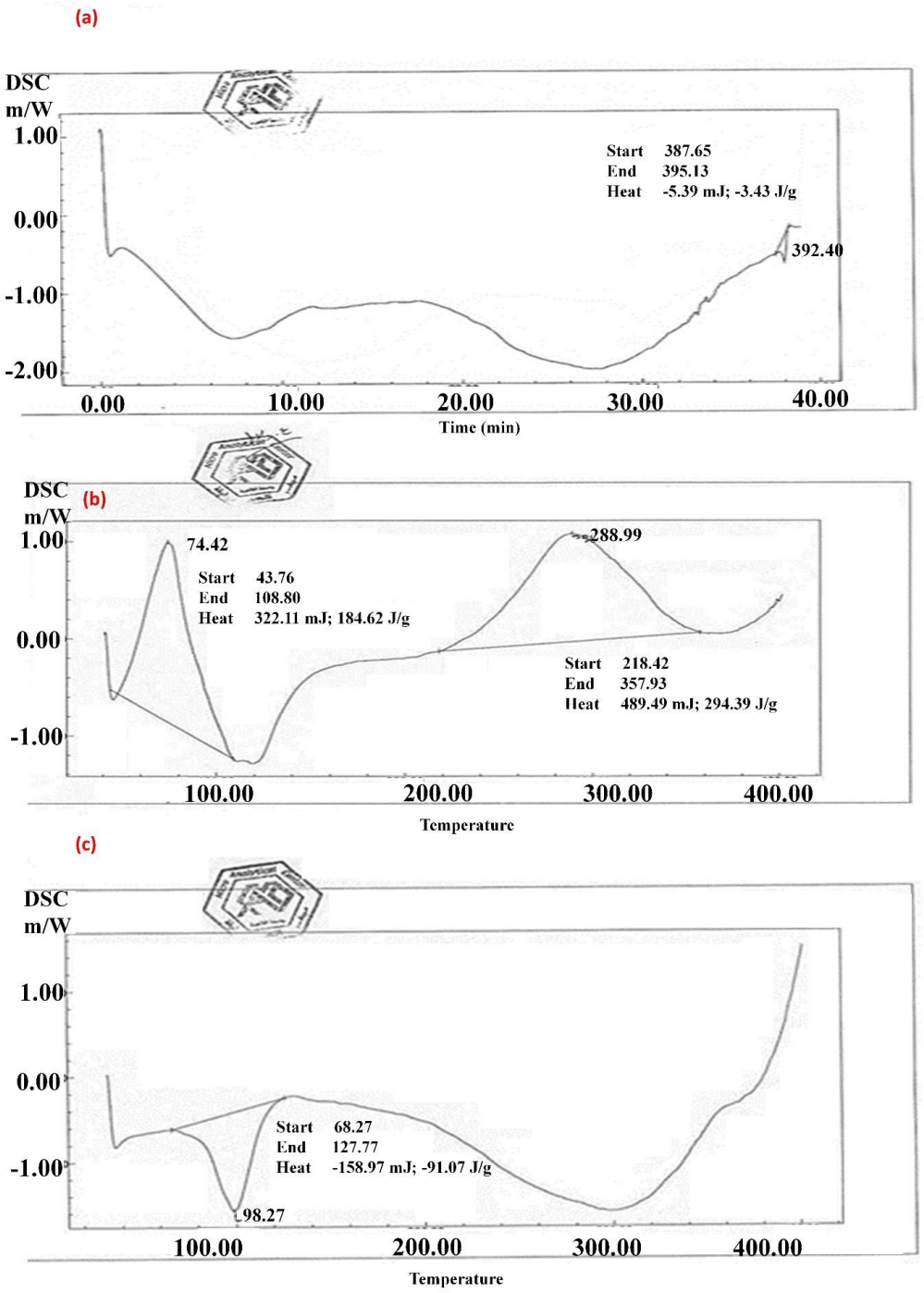

Figure 7. The DSC cure of a) ligand, b) Pt-complex, and c) Pd-complex.

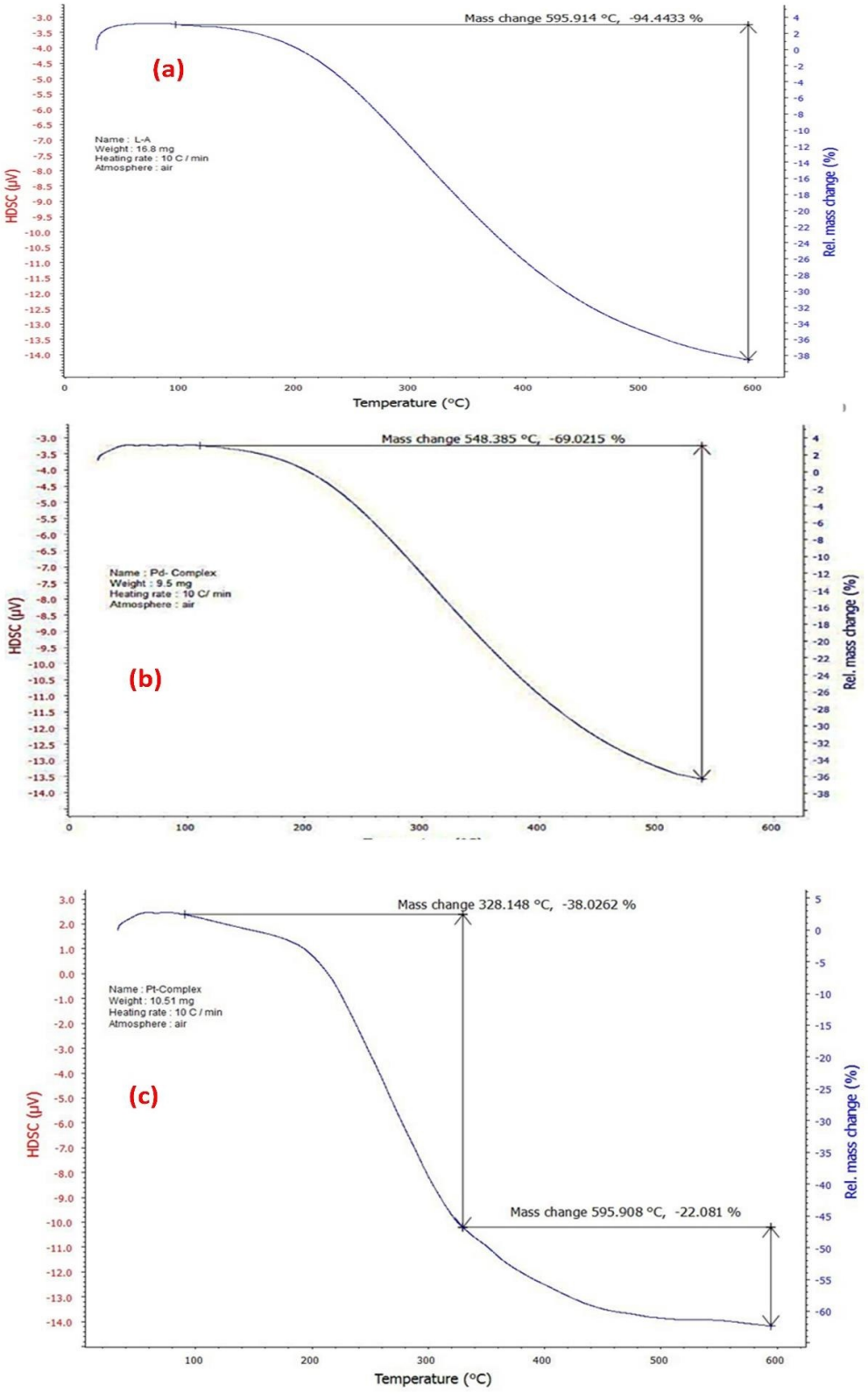

Figure 8. The TGA thermogram of a) ligand, b) Pd-complex, and c) Pt-complex.

designated duration. The resulting plot is denoted as a TGA curve. Schemes 5–7 and Table 4 present coherent findings, affirming the suggested chemical composition of the ligand (H_4-L) and the analyzed complexes, while also providing insights into each pyrolysis phase that transpired.

Based on the data presented in Figure 9, which illustrates the FT-IR spectrum of the ligand (H_4-L), it is possible to infer the formation of the ligand resulting from the interaction between the N-atom of the diazonium salt and the hydroxyl group of 3-hydroxy-acetophenone. This inference is supported by the presence of a distinct absorption band at 1463 cm^{-1}, which confirms the formation of the azo-group (N=N) [48]. Additionally, the absence of an asymmetrical absorption band corresponding to the NH_2 group further reinforces this conclusion. Table 5 provides detailed information on various absorption bands, including notable ones such as the vibrational behavior of the C–H aromatic group at 3120 cm^{-1}, the vibrational behavior of the C–H aliphatic group at 2912 cm^{-1}, the vibrational behavior of the (C=O) group at 1631 cm^{-1}, and a bending absorption band for the CH_3 group at 1400 cm^{-1}. Significantly, the presence of a distinctive peak at 1463 cm^{-1}, which is not observed in the initial substances, can be ascribed to the vibrational motion of the azo-group (N=N). This observation serves as compelling proof for the formation of azo compounds [49]. Figure 9b depicts the nickel complex, showcasing the delicate vibration patterns of the C–H aromatic group at 3190 cm^{-1}. These patterns align with the broad band of the phenolic group (O–H) at 3352 cm^{-1}[41]. Furthermore, there is a noticeable presence of a unique and subtle stretching weak band originating from the C–H aliphatic group at 2927 cm^{-1}. The alterations in the intensities of the azo-bands at 1463 cm^{-1} and 1408 cm^{-1}, potentially indicating coordination with metal ions, are supported by the appearance of a novel Ni–N band at 590 cm^{-1}. The shift of the carbonyl absorption peak from 1610 cm^{-1} in the unbound ligand to a different position indicates coordination with this functional group.

Furthermore, the presence of the Ni–O band at 450 cm^{-1} provides further evidence regarding the coordination between carbonyl and carbinol groups. The analysis of the manganese complex through Fourier-transform infrared (FT-IR) examination reveals several absorption bands related to stretching. A variety of bands can be observed, including the phenolic Ph–OH group, which aligns with the C–H aromatic group and the O–H and aqua groups. Furthermore, the C–H aliphatic group, azo-groups (N=N), carbonyl group (C=O), and carbinol group (C–O) are all linked to various bands. The bands observed correspond to the following wavenumbers: 3415 cm^{-1}, 3178 cm^{-1}, 2900 cm^{-1}, 1462 cm^{-1}, 1409 cm^{-1}, 1608 cm^{-1}, and 1301 cm^{-1} [50]. It should be emphasized that these bands exhibit similarities to those observed in the ligand, albeit with certain alterations in terms of shifting and variations in intensity as a result of the interaction with the metal ion. Furthermore, new bands have been identified, specifically the aqua band H_2O, Mn–N, and Mn–O, which are detailed in Table 5. In the same vein, the platinum complex's FT-IR analysis reveals stretching absorption bands, encompassing a wide band that corresponds to the phenolic group O–H. This band overlaps with both the C–H aromatic group and the O–H group [51].

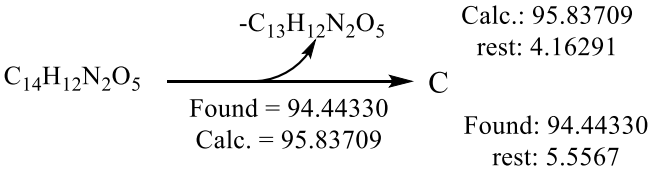

Scheme 5. Decomposition pathway for ligand (H_4L).

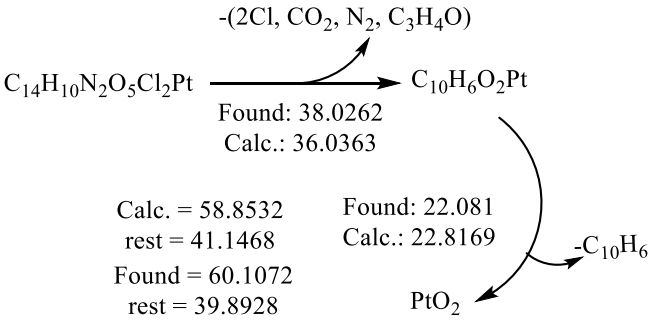

Scheme 6. Decomposition pathway for Pt-complex.

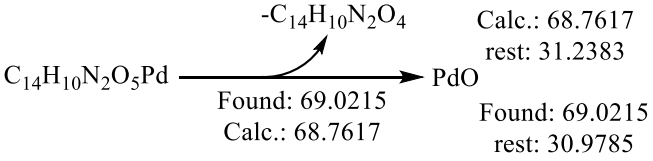

Scheme 7. Decomposition pathway for Pd-complex.

Table 4. Thermogravimetric analysis data for ligand and some complexes.

Entry	Compound (M. wt.)	% Estimated (calculated)		Assignment
		Mass loss	Total mass loss	
1	$C_{14}H_{12}N_2O_5$ (H_4L) 288.26	94.4433 (95.837)	94.4433 (95.837)	$-C_{13}H_{12}N_2O_5$ C
	Calculated: 95.837 % final = 4.16291 %; Estimated 94.4433 % final = 5.5567 %			
2	$C_{14}H_{10}N_2O_5Cl_2Pt$ 391.70	(36.0363) 38.0262 (22.8169) 22.081	60.1072 (58.8532)	-2Cl, CO_2, N_2 $-C_3H_4O$ $-C_{10}H_6$
	Calculated: 58.8532 % final = 41.1468 %; Estimated 60.1072 % final = 39.8928 %			
3	$C_{14}H_{10}N_2O_5Pd$ 392.66	69.0215 (68.7617)	69.0215 (68.7617)	$-C_{14}H_{10}N_2O_4$
	Calculated: 68.7617 % final = 31.2383 %; Estimated 69.0215 % final = 30.9785 %			

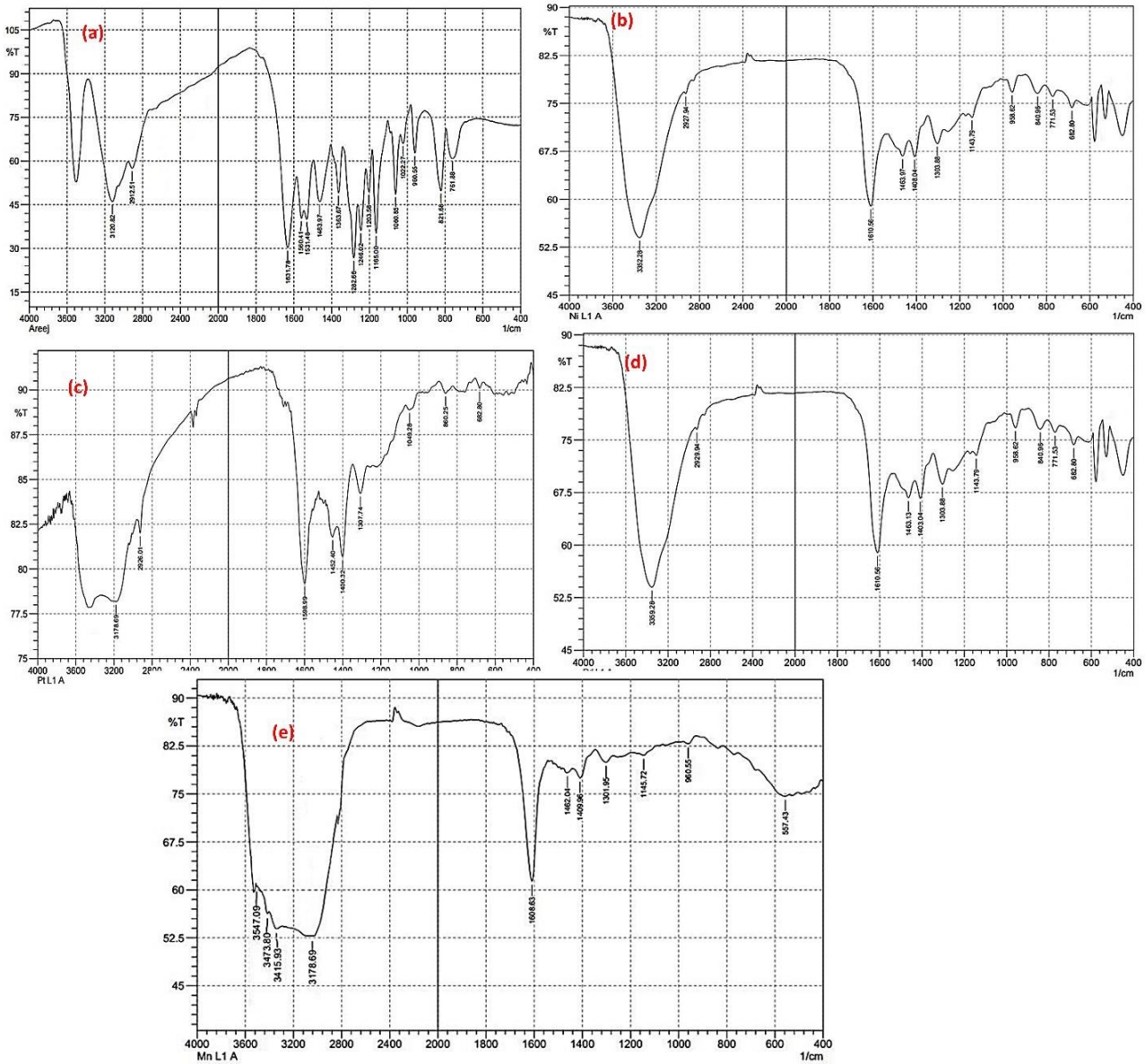

Figure 9. FT-IR spectra of a) ligand, b) Ni-complex, c) Pt-complex, d) Pd-complex, and e) Mn-complex.

Table 5. The IR spectra bands (cm^{-1}) of the ligand and its complexes.

Entry	Compounds	(OH) phenolic	(C–H) aromatic	(C–H) aliphatic	(N=N)	C–O carbinol	(C=O)	M–N (M–O)
1	(H_4L)	3580	3120	2912	1463	1282	1631	–
2	$C_{14}H_{10}N_2O_5Ni$	3352	3190	2927	1463 1408	1303	1610	590 (450)
3	$C_{14}H_{14}N_2O_7Mn$	3415	3178	2900	1462 1409	1301	1608	557 (463)
4	$C_{14}H_{10}N_2O_5Cl_2Pt$	3480	3178	2926	1400 1452	1307	1598	523 (410)
5	$C_{14}H_{10}N_2O_5Pd$	3359	3200	2929	1403 1463	1143	1610	590 (450)

Another bands = H_2O aqua (3473 & 3547) cm^{-1}.

Furthermore, one can observe bands associated with the C–H aliphatic group, azo-group (N=N), carbonyl group (C=O), and carbinol group (C–O). These bands can be detected at the wavenumbers of 3480 cm^{-1}, 3178 cm^{-1}, 2926 cm^{-1}, 1452 cm^{-1}, 1400 cm^{-1}, 1598 cm^{-1}, and 1307 cm^{-1}, respectively. The bands in the ligand exhibit similarities to those found in the manganese complex, albeit with alterations in terms of shifting and variations in intensity as a result of the interaction with the metal ion. Moreover, Table 5 presents the presence of newly identified bands, specifically Pt–N and Pt–O. Furthermore, the palladium complex's FT-IR analysis demonstrates the existence of stretching absorption bands, encompassing a wide band associated with the phenolic group O–H. This specific band exhibits overlap with both the C–H aromatic group and the O–H group. Furthermore, there are bands linked to the C–H aliphatic group, as well as the azo-group (N=N) [52].

3.2 Antioxidant activity of metal complexes

The evaluation of the suppressive impact of ligand H_4L and its metal components, including Mn (II), Ni (II), and Pt (V), on reactive oxygen species was conducted using DPPH. The combination of DPPH with the ligand and its minerals resulted in a change in the color of DPPH from purple to yellow. The change in color occurred due to the transfer of hydrogen from the ligand to the DPPH molecule. The transformation was identified through the utilization of a UV-Vis spectrophotometer with a wavelength of 517 nm. At a 30-minute interval, the inhibitory action of ligand H_4L and its minerals towards reactive oxygen species followed the following order: H_4L > ascorbic acid > Pt-H_2L > Mn-H_2L > Ni-H_2L [44, 53–55]. Previous research has shown that both the ligand and the Platinum complex demonstrated elevated levels of antioxidant activity. The assessment of the antioxidant properties of all the substances using the DPPH radical was conducted by employing the given equation. The outcomes obtained under identical experimental conditions are documented in Table 6 [56, 57].

$$\text{PI}\,\% = \frac{\text{Absorbance of control} - \text{Absorbance of sample}}{\text{Absorbance of control}} \times 100\,\%$$

PI = Percentage Inhibition

$$\text{RSA} = 100 - \text{PI}$$

RSA = Radical Scavenging Activity

3.3 Catalytic investigation of Pd-complex in Suzuki-Miyaura cross-coupling reaction

Initially, the Suzuki-Miyaura cross-coupling reaction involving phenylboronic acid and 4-iodoanisole with a Pd-complex catalyst was chosen as the reference reaction for refining various reaction parameters, including the molar ratio of reactants, choice of base, solvent type, catalyst loading, and reaction temperature (refer to Table 7). The experimental protocol consisted of carrying out the model reaction in the presence of a variety of bases, namely triethylamine, sodium hydroxide, sodium phosphate, sodium carbonate, and potassium carbonate, as indicated in Table 7, entries 1–5. Among the options available, K_2CO_3 was identified as the most effective base. Next, the experimental procedure was carried out with various organic solvents (Table 7, entries 6–10). Within the solvent trials, water (H_2O) emerged as the optimal solvent for the chemical reaction. Throughout these trials, the impact of the solvent on the catalytic performance of the Pd-complex was emphasized, encompassing effects such as solvent influence on reagent solubility, mass transfer, interactions with reactants or products that either enhance or hinder the reaction, selectivity in the reaction, solvent engagement with the catalyst, and stabilization of the transition state. Moreover, the impact of catalyst quantity (refer to Table 7, entries 13, 14) and the stoichiometry of phenylboronic acid and 4-iodoanisole were taken into account as well (refer to Table 7, entries 11, 12). Optimal outcomes were achieved with a ratio of 1.2: 1:2 for (1): (2): base.

After obtaining the optimization results, the extent and applicability of this approach were assessed in the production

Table 6. Radical trapping activities, Percentage Inhibition, and IC_{50} values.

Entry	Compound	Conc. (ppm) µg/mL	PI %	RSA %	IC_{50}
1	$C_{14}H_{12}N_2O_5$ (H_4L)	0.375	9.95	90.05	0.019
		0.186	42.17	57.83	
		0.093	58.99	41.01	
		0.046	66.08	33.92	
2	Mn-H_2L	0.670	62.8	37.52	1.191
		0.335	77.8	22.62	
		0.167	92.2	7.72	
		0.083	89.44	5.86	
3	Ascorbic acid	0.374	12.29	87.80	0.023
		0.186	36.75	63.25	
		0.03	58.74	41.26	
4	Ni-H_2L	2.083	64.8	35.52	1.225
		1.042	79.8	20.62	
		0.521	84.9	15.51	
		0.260	89.8	10.62	
5	Pt-H_2L	0.113	57.8	42.52	1.188
		0.057	72.8	27.62	
		0.028	87.8	12.72	
		0.014	89.4	10.86	

Table 7. Optimization of the reaction conditions for the model reaction of Suzuki-Miyaura cross-coupling reaction[a].

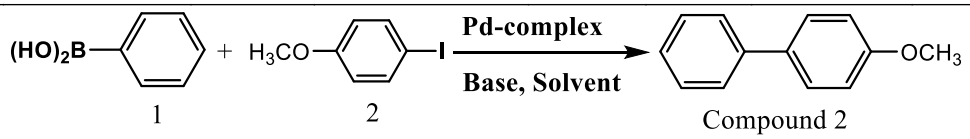

1 2 Compound 2

Entry	Catalyst (mg)	Base	Ratio (1:2:base)	Solvent	T (°C)	Time (min)	Yield (%)[b]
1	50	Et_3N	1.2:1:2	H_2O	Reflux	75	25
2	50	NaOH	1.2:1:2	H_2O	Reflux	60	30
3	50	Na_3PO_4	1.2:1:2	H_2O	Reflux	45	45
4	50	Na_2CO_3	1.2:1:2	H_2O	Reflux	65	30
5	50	K_2CO_3	1.2:1:2	H_2O	Reflux	15	96
6	50	K_2CO_3	1.2:1:2	EtOH	Reflux	30	70
7	50	K_2CO_3	1.2:1:2	DMF	Reflux	25	75
8	50	K_2CO_3	1.2:1:2	MeOH	Reflux	40	65
9	50	K_2CO_3	1.2:1:2	CH_2Cl_2	Reflux	70	45
10	50	K_2CO_3	1.2:1:2	NMP[c]	Reflux	20	75
11	50	K_2CO_3	1.2:1:1.5	H_2O	Reflux	30	65
12	50	K_2CO_3	1:1:2	H_2O	Reflux	30	65
13	40	K_2CO_3	1.2:1:2	H_2O	Reflux	45	70
14	60	K_2CO_3	1.2:1:2	H_2O	Reflux	20	95

a) General reaction conditions: compound (1) (x mmol), compound (2) (y mmol), base (z mmol), solvent (6 mL).
b) Isolated yields.
c) N-methylpyrrolidone.

of various biaryl compounds. This was achieved by employing different substrates that contained I, Br, and/or Cl, and reacting them with phenylboronic acid (Table 8). The efficiency of the Pd-complex has been noted in its ability to catalyze a wide range of aryl halides (X = Cl, Br, I) containing both electron-donating and electron-withdrawing groups. Initially, the responses of aryl iodides were examined, resulting in favorable yields. In contrast to aryl iodide, the utilization of aryl bromides as substrates led to a decreased product yield. The decreased yield can be ascribed to the slower oxidation-addition process observed with aryl bromide when compared to aryl iodide. When aryl chloride is present, the reactivity is reduced compared to that of iodo and bromo derivatives.

The primary consideration in catalysis reactions is the ability to reuse the catalyst. In order to assess the reusability of the palladium complex, an experiment was conducted using the Suzuki reaction with 4-iodoanisole, phenylboronic acid, K_2CO_3, and a Pd-complex in a 3 mL water solution at reflux temperature in the presence of air. The catalytic activity of the catalyst remains unaffected even after being reused for four cycles. The leaching of Pd was quantified through ICP analysis (Run 1: 96 %, 15 min; Run 2: 93 %, 25 min; Run 3: 89 %, 30 min; Run 4: 88 %, 45 min).

The optimized configuration, atom dot representation, molecular orbital, and overall charge distribution for the Pt-complex, Ni-complex, Pd-complex, and Mn-complex compounds are displayed in Figures 10 to 13, respectively. Moreover, more data for stretch, bend, stretch-bend, torsion, Non-1,4-VDW, 1,4-VDW, dipole-dipole interaction, and total energy (kcal/mol) regarding Ni-complex and Pd-complex were provided in Table 9.

Table 8. Investigation and applicability of Pd-complex in Suzuki-Miyaura cross-coupling reaction[a].

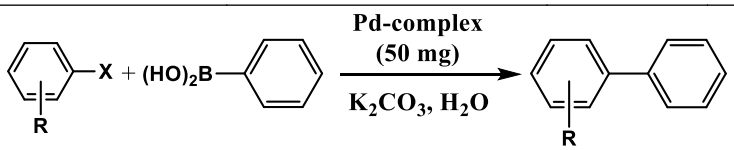

Entry	Substrate	Final Product	Time (min)	Yield (%)[b]
1	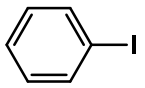	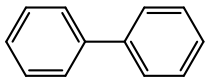 **Compound 1**	20	94
2	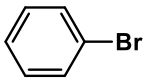	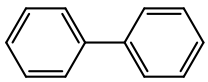 **Compound 1**	35	92
3	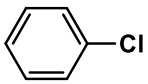	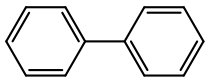 **Compound 1**	70	89
4	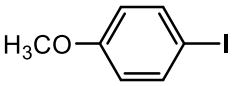	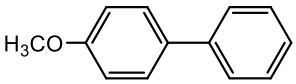 **Compound 2**	15	96
5	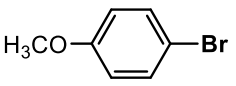	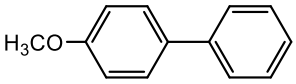 **Compound 2**	30	96
6	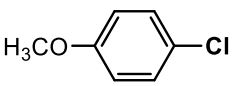	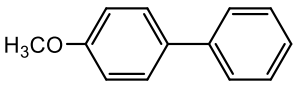 **Compound 2**	65	92
7	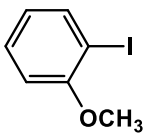	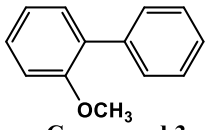 **Compound 3**	25	90

Continued on next page

Table 8. Investigation and applicability of Pd-complex in Suzuki-Miyaura cross-coupling reaction[a]. (Continued)

Entry	Substrate	Final Product	Time (min)	Yield (%)[b]
8	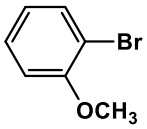	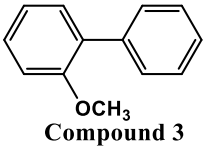 **Compound 3**	45	87
9	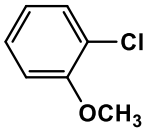	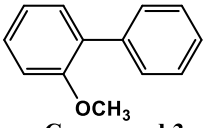 **Compound 3**	90	86
10	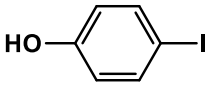	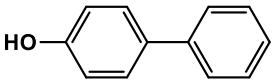 **Compound 4**	20	95
11	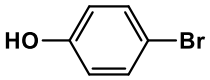	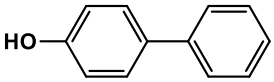 **Compound 4**	25	94
12	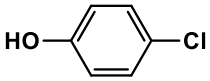	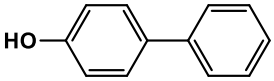 **Compound 4**	40	90
13	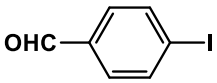	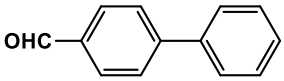 **Compound 5**	40	86
14	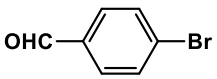	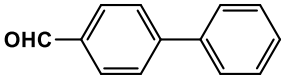 **Compound 5**	65	82
15	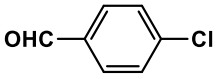	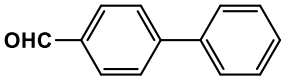 **Compound 5**	90	79

a) Reaction conditions: aryl halide (5.0 mmol), phenylboronic acid (6.0 mmol), K_2CO_3 (10.0 mmol), H_2O (6.0 mL), reflux.
b) Isolated Yields.

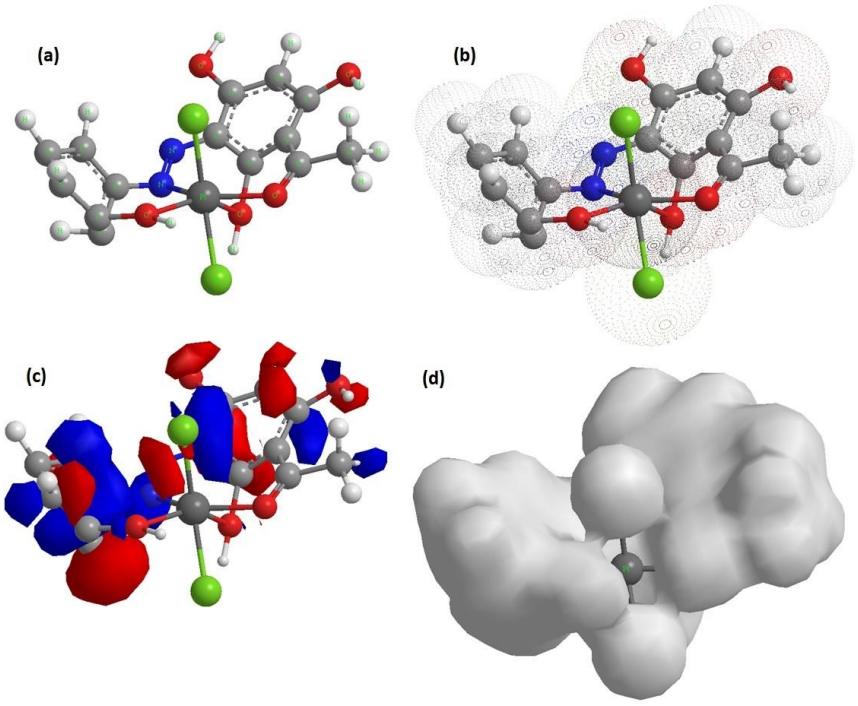

Figure 10. Application of computational chemistry for Pt-complex a) energy optimized structure of Pt-complex structure by DFT calculation at the B3LYP/6-31G* level, b) the atom dot mapping for Pt-complex, c) The molecular orbital for Pt-complex, and d) The total charge density for Pt-complex.

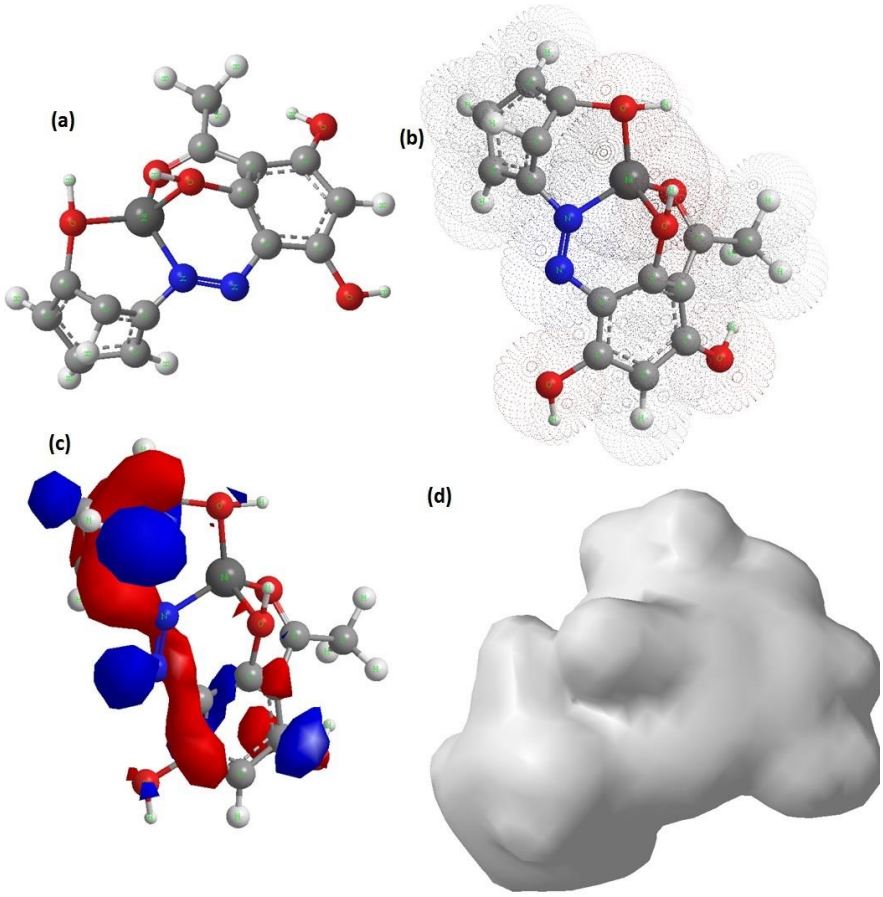

Figure 11. Application of computational chemistry for Ni-complex a) energy optimized structure of Ni-complex structure by DFT calculation at the B3LYP/6-31G* level, b) the atom dot mapping for Ni-complex, c) The molecular orbital for Ni-complex, and d) The total charge density for Ni-complex.

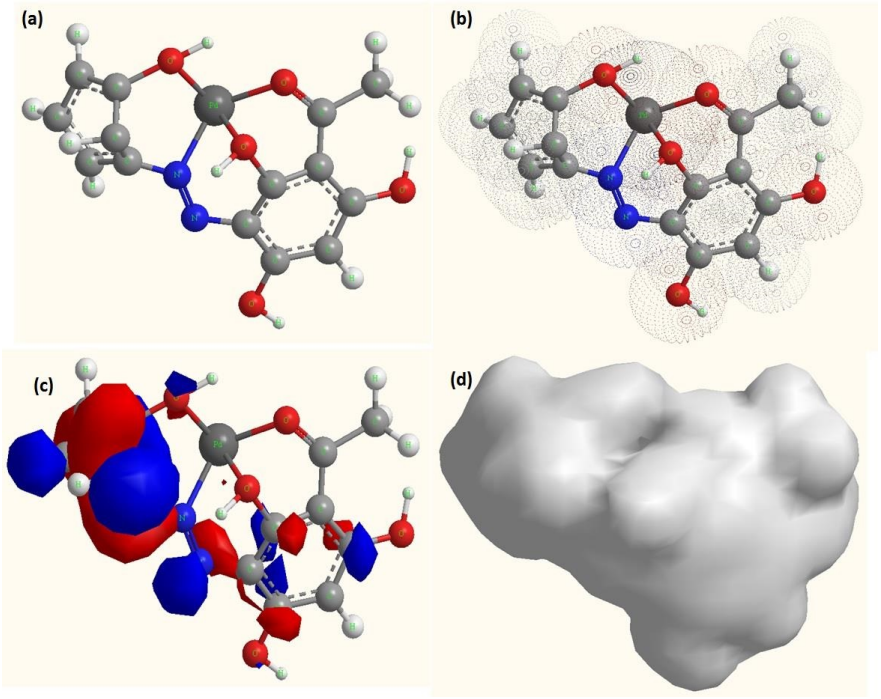

Figure 12. Application of computational chemistry for Pd-complex a) energy optimized structure of Pd-complex structure by DFT calculation at the B3LYP/6-31G* level, b) the atom dot mapping for Pd-complex, c) The molecular orbital for Pd-complex, and d) The total charge density for Pd-complex.

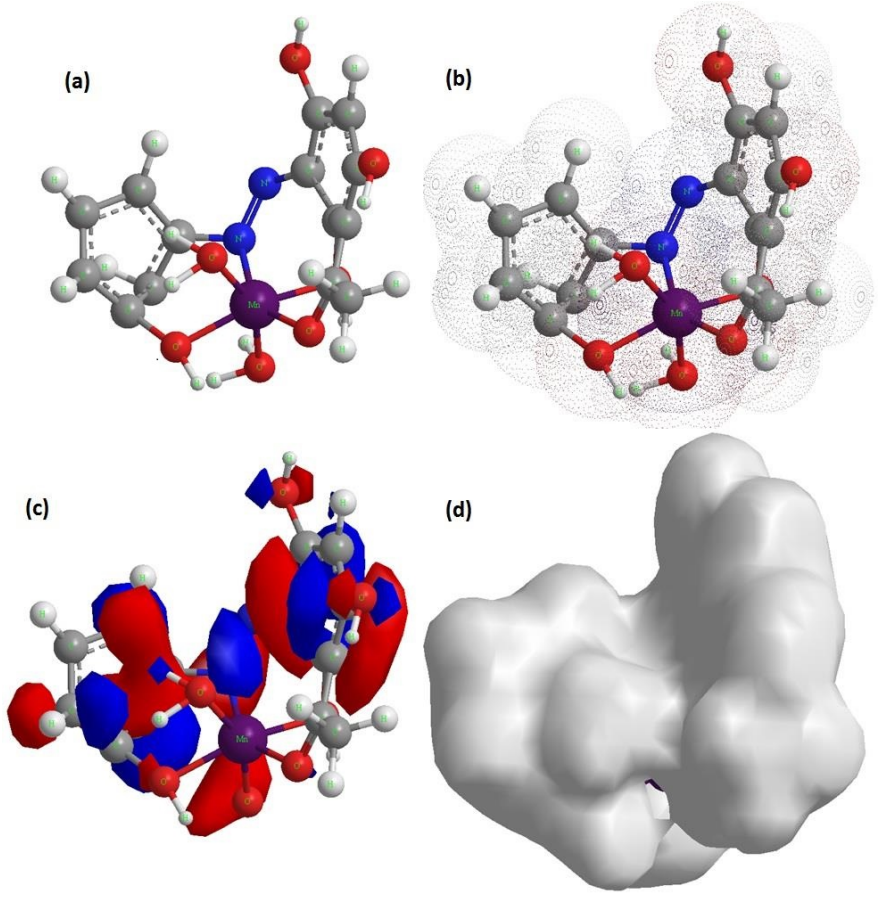

Figure 13. Application of computational chemistry for Mn-complex a) energy optimized structure of Mn-complex structure by DFT calculation at the B3LYP/6-31G* level, b) the atom dot mapping for Mn-complex, c) The molecular orbital for Mn-complex, and d) The total charge density for Mn-complex.

Table 9. More DFT data for Ni and Pd complex.

Entry	Name	Pd-complex	Ni-complex
1	Stretch	50.5010	37.5929
2	Bend	974.1223	969.5097
3	Stretch-Bend	−5.1879	−1.9725
4	Torsion	168.8052	214.7243
5	Non-1,4-VDW	−4.2382	−5.2505
6	1,4-VDW	46.8684	34.6251
7	Dipole/Dipole	−0.3856	0.7575
8	Total Energy	1230.4852 kcal/mol	1249.9864 kcal/mol

4. Conclusion

The synthesis of the azo-ligand denoted as (E)-1-(2,4,6-trihydroxy-3-((3-hydroxyphenyl) diazinyl)phenyl)ethan-1-one (H_4L) was effectively conducted using diazotization and coupling techniques. Subsequently, the ligand was reacted with different metal ions such as Ni (II), Pt (IV), Pd (II), and Mn (II) individually, resulting in the formation of stable complexes. The coordination of the metal ions occurred via the oxygen and nitrogen atoms of the azo-group present in the ligand (H_4L), as confirmed by FT-IR analysis which revealed the presence of M−O and M−N bands, along with shifts in carbinol and carbonyl absorption bands indicating coordination through these functional groups. Some complexes also exhibited binding with aqua water molecules as indicated by the spectra. Electronic spectra and molar conductivity measurements were utilized to determine the geometry of the complexes, which were found to be either octahedral or tetrahedral. LC-Mass spectra, fragmentation patterns of the complexes, and elemental analysis provided insight into the molecular formulas of the complexes. Thermal analysis of certain compounds further supported the presence or absence of water molecules within the complexes. Moreover, the antioxidant activity of the compounds against DPPH was evaluated, with results showing that (H_4L > ascorbic acid > Pt-H_2L > Mn-H_2L > Ni-H_2L) after 30 minutes, indicating that the ligand and Platinum complex exhibited higher antioxidant efficacy. Additionally, the Pd-complex demonstrated successful application in the Suzuki-Miyauara cross-coupling reaction.

Authors Contributions
This project was carried out collaboratively by all authors. AAS participated in examining the samples and analysing the data. AMA prepared the samples, wrote, and edited the manuscript.

Availability of Data and Materials
The data that support the findings of this study are available from the corresponding author upon reasonable request.

Conflict of Interests
The authors declare that they have no known competing financial interests or personal relationships that could have appeared to influence the work reported in this paper.

References

[1] C.C.C. Johansson Seechurn, M.O. Kitching, T.J. Colacot, and V. Snieckus. *Angew. Chem. Int. Ed.*, **51**(2012):5062–5085. DOI: https://doi.org/10.1002/anie.201107017.

[2] D. Astruc. *Anal. Bioanal. Chem.*, **399**(2011): 1811–1814. DOI: https://doi.org/10.1007/s00216-010-4555-1.

[3] S. Clair and D.G. de Oteyza. *Chem. Rev.*, **119**(2019):4717–4776. DOI: https://doi.org/10.1021/acs.chemrev.8b00601.

[4] Z. Bao, W.K. Chan, and L. Yu. *J. Am. Chem. Soc.*, **117**(1995):12426–12435. DOI: https://doi.org/10.1021/ja00155a007.

[5] S. Kotha, K. Lahiri, and D. Kashinath. *Tetrahedron*, **58**(2002):9633–9695. DOI: https://doi.org/10.1016/S0040-4020(02)01188-2.

[6] R. Martin and S.L. Buchwald. *Acc. Chem. Res.*, **41**(2008):1461–1473. DOI: https://doi.org/10.1021/ar800036s.

[7] S.E. Hooshmand, B. Heidari, R. Sedghi, and R.S. Varma. *Green Chem.*, **21**(2019):381–405. DOI: https://doi.org/10.1039/C8GC02860E.

[8] G.A. Molander and C.R. Bernardi. *J. Org. Chem.*, **67**(2002):8424–8429. DOI: https://doi.org/10.1021/jo026236y.

[9] V. Polshettiwar, A. Decottignies, C. Len, and A. Fihri. *ChemSusChem*, **3**(2010):502–522. DOI: https://doi.org/10.1002/cssc.200900221.

[10] F.-S. Han. *Chem. Soc. Rev.*, **42**(2013):5270–5298. DOI: https://doi.org/10.1039/C3CS35521G.

[11] H.C. Brown and B. Singaram. *Pure Appl. Chem.*, **59**(1987):879–894. DOI: https://doi.org/10.1351/pac198759070879.

[12] A. Das and T.K. Panda. *ChemCatChem*, **15**(2023):e202201011. DOI: https://doi.org/10.1002/cctc.202201011.

[13] Y.L. Phang, J.-K. Jin, F.-L. Zhang, and Y.-F. Wang. *Chem. Commun.*, **60**(2024):4275–4289. DOI: https://doi.org/10.1039/D4CC00398E.

[14] Y. Zhang, X. Zhang, and Q. Yan. *J. Org. Chem.*, **88**(2023):10609–10616. DOI: https://doi.org/10.1021/acs.joc.3c00629.

[15] K. Kang, L. Huang, and D.J. Weix. *J. Am. Chem. Soc.*, **142**(2020):10634–10640. DOI: https://doi.org/10.1021/jacs.0c04670.

[16] V.M. Chernyshev and V.P. Ananikov. *ACS Catal.*, **12**(2022):1180–1200. DOI: https://doi.org/10.1021/acscatal.1c04705.

[17] L. Nan, C. Yalan, L. Jixiang, O. Dujuan, D. Wenhui, J. Rouhi, and M. Mustapha. *RSC Adv.*, **10**(2020):27923–27931. DOI: https://doi.org/10.1039/D0RA03915B.

[18] V.B. Phapale and D.J. Cárdenas. *Chem. Soc. Rev.*, **38**(2009):1598–1607. DOI: https://doi.org/10.1039/B805648J.

[19] C. Chen, K. Tagami, and Y. Kishi. *J. Org. Chem.*, **60**(1995):5386–5387, . DOI: https://doi.org/10.1021/jo00122a011.

[20] J. Terao, H. Watanabe, A. Ikumi, H. Kuniyasu, and N. Kambe. *J. Am. Chem. Soc.*, **124**(2002):4222–4223. DOI: https://doi.org/10.1021/ja025828v.

[21] R.D.J. Froese, C. Lombardi, M. Pompeo, R.P. Rucker, and M.G. Organ. *Acc. Chem. Res.*, **50**(2017):2244–2253. DOI: https://doi.org/10.1021/acs.accounts.7b00249.

[22] Y. Han, H.V. Huynh, and G.K. Tan. *Organometallics*, **26**(2007):6447–6452. DOI: https://doi.org/10.1021/om700753d.

[23] C.M. Crudden and D.P. Allen. *Coord. Chem. Rev.*, **248**(2004):2247–2273. DOI: https://doi.org/10.1016/j.ccr.2004.05.013.

[24] K. Sayin, S.E. Kariper, M. Taştan, T.A. Sayin, and D. Karakaş. *J. Mol. Struct.*, **1176**(2019):478–487. DOI: https://doi.org/10.1016/j.molstruc.2018.08.103.

[25] S. Çekirdek, S. Yaşar, and İ. Özdemir. *Appl. Organomet. Chem.*, **28**(2014):423–431. DOI: https://doi.org/10.1002/aoc.3143.

[26] M. Ashraf, M.S. Ahmad, Y. Inomata, N. Ullah, M.N. Tahir, and T. Kida. *Coord. Chem. Rev.*, **476**(2023):214928. DOI: https://doi.org/10.1016/j.ccr.2022.214928.

[27] A.K. King, A. Brar, G. Li, and M. Findlater. *Organometallics*, **42**(2023):2353–2358. DOI: https://doi.org/10.1021/acs.organomet.3c00231.

[28] X. Li, Z. Zhou, Y. Wang, J. Dong, X. Jia, Z. Hu, Q. Wei, W. Zhang, Y. Jiang, J. Zhang, and Y. Dong. *Int. J. Biol. Macromol.*, **233**(2023):123596. DOI: https://doi.org/10.1016/j.ijbiomac.2023.123596.

[29] S. Ji, X. Lu, M. Zhang, L. Leng, H. Liu, K. Yin, C. Xu, C. He, J.H. Horton, J. Zhang, and Z. Li. *Chem. Eng. J.*, **452**(2023):139205. DOI: https://doi.org/10.1016/j.cej.2022.139205.

[30] M. Gao, J. Wang, W. Shang, Y. Chai, W. Dai, G. Wu, N. Guan, and L. Li. *Catal. Today*, **410**(2023):237–246. DOI: https://doi.org/10.1016/j.cattod.2022.02.011.

[31] S. Payamifar, M. Abdouss, and A. Poursattar Marjani. *Appl. Organomet. Chem.*, **38**(2024):e7458. DOI: https://doi.org/10.1002/aoc.7458.

[32] K.R. Chaudhari, A.P. Wadawale, A.K. Pathak, and S. Dey. *Inorg. Chem.*, **63**(2024):1427–1438. DOI: https://doi.org/10.1021/acs.inorgchem.3c03963.

[33] M. Mirza-Aghayan, M. Heidarian, and M. Alizadeh. *J. Organomet. Chem.*, **1009**(2024):123079. DOI: https://doi.org/10.1016/j.jorganchem.2024.123079.

[34] B. Tahmasbi, M. Darabi, and M. Nikoorazm. *Appl. Organomet. Chem.*, **38**(2024):e7348. DOI: https://doi.org/10.1002/aoc.7348.

[35] T. Chen, Y. Pang, S.H. Ali, L. Chen, Y. Li, X. Yan, and B. Wang. *Molecular Catalysis*, **558**(2024):114045, . DOI: https://doi.org/10.1016/j.mcat.2024.114045.

[36] S.H. Jawad and K.J. Al-Adilee. *J. Mol. Struct.*, **1277**(2023):134846, . DOI: https://doi.org/10.1016/j.molstruc.2022.134846.

[37] S.H. Jawad and K.J. Al-Adilee. *Results in Chemistry*, **4**(2022):100573, . DOI: https://doi.org/10.1016/j.rechem.2022.100573.

[38] K.J. Al-Adilee, S.H. Jawad, H.A.K. Kyhoiesh, and H.M. Hassan. *J. Mol. Struct.*, **1295**(2024):136695. DOI: https://doi.org/10.1016/j.molstruc.2023.136695.

[39] A. Ali Salih Al-Hamdani, T. AM Al-Alwany, M. Abdulameer Mseer, A. Malek Fadhel, and Y. F Al-Khafaji. *Egyptian Journal of Chemistry*, **66**(2023):223–235. DOI: https://doi.org/10.21608/ejchem.2022.144403.6297.

[40] H.S. Al-Atbi, B.K. Al-Salami, and I.J. Al-Assadi. *Journal of Physics: Conference Series*, **1294**(2019): 052033. DOI: https://doi.org/10.1088/1742-6596/1294/5/052033.

[41] R.K.H. Al-Daffay and A.A.S. Al-Hamdani. *Baghdad Science Journal*, **20**(2023):0121. DOI: https://doi.org/10.21123/bsj.2022.6709.

[42] K.T. Mahmudov, A.V. Gurbanov, V.A. Aliyeva, G. Resnati, and A.J.L. Pombeiro. *Coord. Chem. Rev.*, **418**(2020):213381. DOI: https://doi.org/10.1016/j.ccr.2020.213381.

[43] V.T. Suleman, A.A.S. Al-Hamdani, S.D. Ahmed, V.Y. Jirjees, M.E. Khan, A. Dib, W. Al Zoubi, and Y.G. Ko. *Appl. Organomet. Chem.*, **34**(2020):e5546. DOI: https://doi.org/10.1002/aoc.5546.

[44] M.J. Kareem, A.A.S. Al-Hamdani, V.Y. Jirjees, M.E. Khan, A.W. Allaf, and W. Al Zoubi. *J. Phys. Org. Chem.*, **34**(2021):e4156. DOI: https://doi.org/10.1002/poc.4156.

[45] A.A.S. Al-Hamdani, A.M. Balkhi, A. Falah, and S.A. Shaker. *J. Saudi Chem. Soc.*, **20**(2016):487–501. DOI: https://doi.org/10.1016/j.jscs.2012.08.001.

[46] N. Mohamed Wannas, A.A.S. Al-Hamdani, and W. Al Zoubi. *J. Phys. Org. Chem.*, **33**(2020):e4099. DOI: https://doi.org/10.1002/poc.4099.

[47] R.K. Al-Daffaay. *Baghdad Science Journal*, **19**(2022):1036–1036. DOI: https://doi.org/10.21123/bsj.2022.6162.

[48] M. Ali Dahi and A.J. Jarad. *Journal of Physics: Conference Series*, **1664**(2020):012090. DOI: https://doi.org/10.1088/1742-6596/1664/1/012090.

[49] W. Al Zoubi, A.A.S. Al-Hamdani, S. Duraid Ahmed, H.M. Basheer, R.S.A. Al-Luhaibi, A. Dib, and Y.G. Ko. *J. Phys. Org. Chem.*, **32**(2019):e3916, . DOI: https://doi.org/10.1002/poc.3916.

[50] S.M.H. Obaid, A.J. Jarad, and A.A. Salih Al-Hamdani. *Journal of Physics: Conference Series*, **1660**(2020): 012028. DOI: https://doi.org/10.1088/1742-6596/1660/1/012028.

[51] A.A.S. Al-Hamdani and M.Q. Abdulridha. *Baghdad Science Journal*, **20**(2023):1964–1975. DOI: https://doi.org/10.21123/bsj.2023.7629.

[52] W. Al Zoubi, S.G. Mohamed, A.A.S. Al-Hamdani, A.P. Mahendradhany, and Y.G. Ko. *RSC Adv.*, **8**(2018):23294–23318, . DOI: https://doi.org/10.1039/C8RA01890A.

[53] M.B. Halli, Shashidhar, and Z.S. Qureshi. *Synth. React. Inorg. Met.-Org. Chem.*, **34**(2004):1755–1768. DOI: https://doi.org/10.1081/SIM-200030199.

[54] S.A. Jaber, H.A.K. Kyhoiesh, and S.H. Jawad. *Journal of Physics: Conference Series*, **1818**(2021): 012013. DOI: https://doi.org/10.1088/1742-6596/1818/1/012013.

[55] I.P. Ejidike and P.A. Ajibade. *Bioinorg. Chem. Appl.*, **2015**(2015):890734. DOI: https://doi.org/10.1155/2015/890734.

[56] O.A. El-Gammal, F.S. Mohamed, G.N. Rezk, and A.A. El-Bindary. *J. Mol. Liq.*, **326**(2021):115223. DOI: https://doi.org/10.1016/j.molliq.2020.115223.

[57] V.Y. Jirjees, A.A.S. Al-Hamdani, N.M. Wannas, F.A. R, A. Dib, and W. Al Zoubi. *J. Phys. Org. Chem.*, **34**(2021):e4169. DOI: https://doi.org/10.1002/poc.4169.